Published in final edited form as:
Exp Neurol. 2014 November ; 261: 757–771. doi:10.1016/j.expneurol.2014.08.015.

Osteopontin Expression in Acute Immune Response Mediates Hippocampal Synaptogenesis and Adaptive Outcome Following Cortical Brain Injury

Julie L. Chan, **Thomas M. Reeves**, and **Linda L. Phillips**
Department of Anatomy and Neurobiology, Virginia Commonwealth University, P.O. Box 980709 Richmond, VA 23298

Abstract

Traumatic brain injury (TBI) produces axotomy, deafferentation and reactive synaptogenesis. Inflammation influences synaptic repair, and the novel brain cytokine osteopontin (OPN) has potential to support axon regeneration through exposure of its integrin receptor binding sites. This study explored whether OPN secretion and proteolysis by matrix metalloproteinases (MMPs) mediate the initial degenerative phase of synaptogenesis, targeting reactive neuroglia to affect successful repair. Adult rats received unilateral entorhinal cortex lesion (UEC) modeling adaptive synaptic plasticity. Over the first week postinjury, hippocampal OPN protein and mRNA were assayed and histology performed. At 1–2d, OPN protein increased up to 51 fold, and was localized within activated, mobilized glia. OPN transcript also increased over 50 fold, predominantly within reactive microglia. OPN fragments known to be derived from MMP proteolysis were elevated at 1d, consistent with prior reports of UEC glial activation and enzyme production. Postinjury minocycline immunosuppression attenuated MMP-9 gelatinase activity, which was correlated with reduction of neutrophil gelatinase-associated lipocalin (LCN2) expression, and reduced OPN fragment generation. The antibiotic also attenuated removal of synapsin-1 positive axons from the deafferented zone. OPN KO mice subjected to UEC had similar reduction of hippocampal MMP-9 activity, as well as lower synapsin-1 breakdown over the deafferented zone. MAP1B and N-cadherin, surrogates of cytoarchitecture and synaptic adhesion, were not affected. OPN KO mice with UEC exhibited time dependent cognitive deficits during the synaptogenic phase of recovery. This study demonstrates that OPN can mediate immune response during TBI synaptic repair, positively influencing synapse reorganization and functional recovery.

Introduction

Axotomy is a principal pathology generated by traumatic brain injury (TBI), resulting in synaptic deafferentation (Povlishock and Katz, 2005), and inducing synapse reorganization

Corresponding Author: Dr. Linda L. Phillips, Department of Anatomy and Neurobiology, Virginia Commonwealth University, P.O. Box 980709, Richmond, VA 23298, 804-828-9657, llphilli@vcu.edu.

at sites of terminal loss (Steward, 1989). Two mechanisms controlling reinnervation are acute inflammation (Correale and Villa, 2004; Lucas et al., 2006), and activation of extracellular matrix (ECM) molecules surrounding synapses (Venstrom and Reichardt, 1993; Dityatev and Schachner, 2003). Acute postinjury inflammation activates local glia to remove degenerated axons, as well as provides growth factors for axon sprouting and repopulation of postsynaptic sites. Surrounding ECM forms the environment where immune molecules operate, and stabilizes synaptic structure (Ruoslahti, 1996; Dityatev and Schachner, 2006). Matrix metalloproteinases (MMPs) are secreted into this space, targeting both structural and immune proteins during reactive synaptogenesis, and influencing synapse regeneration (Ethel and Ethell, 2007; Verslegers et al, 2013).

Among immune mediators of synaptogenic onset, both chemokines and cytokines are critical (Shohami et al., 1994; Morganti-Kossmann et al., 2002). Interleukins are prominent, and garner significant investigation, both in experimental TBI and clinically (Knoblach and Faden, 1998; Shohami et al., 1997; Rothwell and Luheshi, 2000; Csuka et al., 1999). Recently, a novel cytokine, osteopontin (OPN), was localized in traumatized cortex (Shin et al., 2005; Plantman, 2012), and found upregulated postinjury (von Gertten et al., 2005; Cernak et al., 2011). OPN is relevant to synaptogenesis because it contains RGD and SVVYGLR integrin receptor binding sequences, consistent with a chemotactic role in microglial activation. Such activation includes cell migration, shifts in functional status, and the synthesis of cytokines and MMPs capable of further stimulating neuroglia during synapse reformation (Kumar et al., 2013; Hanisch, 2002; del Zoppo et al., 2012; Lively and Schlichter, 2013). Importantly, MMP lysis exposes these RGD/SVVYGLR sequences, generating integrin binding OPN fragments which stimulate reactive microglia and astrocytes (Ellison et al., 1998; Shin et al., 2005; Kang et al., 2008). While MMPs alter CNS plasticity in a time dependent fashion (Goussev et al., 2003; Falo et al., 2006; Warren et al., 2012), the significance of such OPN fragment production during synaptogenesis is not understood. This interaction suggests that MMP OPN processing within the synaptogenic environment supports cell signaling for ECM boundary formation, guiding debris clearance and axonal-dendritic regeneration.

The present study examined time dependent OPN/MMP response during deafferentation induced synaptogenesis in the unilateral entorhinal cortical lesion (UEC) model of adaptive synaptic recovery, (Phillips et al., 1994). It was hypothesized that deafferentation acutely elevates OPN, stimulating increase in MMP-generated fragments and targeted effects on surrounding glia mediating the onset of synaptogenesis. OPN protein and mRNA expression, histological localization, and MMP enzyme activity, were assessed during the first week postinjury to determine whether OPN response is related to glial and synaptic change in initial phase of the recovery process. The immunosuppressant minocycline was applied to attenuate this glial response, measuring OPN expression and assessing synaptic reorganization. Using OPN KO mice, we explored if OPN loss affected structural or functional recovery after UEC. Our results support OPN as an important mediator of cell response during the early stages of reactive synaptogenesis.

Materials and Methods

Experimental Animals

All procedures met national guidelines for care and use of laboratory animals, and all experimental protocols were approved by the VCU Institutional Animal Care and Use Committee. Both rats and mice subjects were utilized. Male Sprague Dawley rats (300–350 g; Harlan Laboratories) were housed in pairs under a temperature (22°C) and humidity controlled environment with food and water *ad libitum*, and subjected to a 12 hour dark-light cycle. Rats were subjected to unilateral entorhinal lesioned (UEC; n=62) and randomly assigned to subgroups which were evaluated at 1–7d postinjury by either Western Blot (WB), immunohistochemistry (IHC), qRT-PCR, in situ hybridization (ISH) or gelatin zymography methods. For the minocycline experiments, rats were randomly assigned to lesioned saline-treated or lesioned drug-treated groups, and evaluated at 2d postinjury by either WB or IHC (n=16). For all analyses, the matched contralateral uninjured brain region served as control.

A second set of experiments used male WT C57BL/6J or OPN KO mice (B6.129S6 (Cg)-Spp1^{tm1Blh}/J) (20–30 g; 8–11 weeks old; The Jackson Laboratory, Bar Harbor, ME) housed under the same environmental conditions as rat subjects. For molecular assessments, WT or OPN KO mice were randomly selected, subjected to UEC, and evaluated at 2d postinjury by WB, IHC, or gelatin zymography (n=40 each strain; total n= 80). For behavioral analysis, WT and OPN KO mice were randomly assigned to an uninjured or UEC group and evaluated using the novel object recognition (NOR) task at 4, 7, 14, 21, and 28d postinjury before being sacrificed (n=48). For molecular analyses, the matched contralateral uninjured brain region served as control for UEC lesion effects, and WT versus OPN KO compared for experimental effect. Uninjured mice served as controls for NOR behavioral analyses.

Unilateral Entorhinal Cortex Lesion: Rat and Mouse

The rat UEC protocol was a modification of that described by Loesche and Steward (1977). Rats were anesthetized with 4% isoflurane in carrier gas of 70% N_2O, 30% O_2 for 4 min, heads shaved, then maintained on 2% isoflurane in carrier gas of 70% N_2O, 30% O_2 delivered via nose cone during surgery. Body temperature was maintained at 37°C by heating pad (Harvard Apparatus, Holliston, MA), and heart rate (bpm), arterial oxygen saturation (percent O_2), breath rate (brpm), pulse/breath distention (μm) were monitored by pulse oximetry (MouseOx; Starr Life Sciences, Oakmont, PA). Anesthetized rats were secured in a stereotaxic device, a midline incision and 2 mm craniectomy performed to visualize intact dura mater above the right entorhinal cortex (EC). Electrolytic lesions were delivered through Teflon®-coated wire penetrating the dura and transmitting 1.5 mA for 40 s to 8 stereotaxic coordinates: 10° lateral to perpendicular; 1.5 mm rostral to the transverse sinus; 3 and 4 mm lateral to the midline at 6, 4, and 2 mm ventral to the brain surface; and a third, 5 mm lateral at 4 and 2 mm ventral to the brain surface. After lesion, electrode was removed, incision sutured and topical anesthetic/antibiotic applied. Animals were housed singly in a warm chamber during post-operative recovery and monitored for discomfort or distress before being returned to home cages.

The mouse UEC protocol was a modification of the Hardman et al., method (1997). Mice were anesthetized, body temperature maintained and vital physiology monitored as described for rat subjects. Under anesthesia, mice were secured in a stereotaxic device and dura mater above the right EC exposed. Electrolytic lesions were delivered by Teflon®-coated wire penetrating the dura and transmitting 2.0 mA for 15 s to 3 coordinates: 10° lateral to perpendicular; 0.5 mm rostral to the lamdoidal suture; 2 and 3 mm lateral to the midline at 3.5 mm ventral to the brain surface; and 3.5 mm lateral at 3.0 mm ventral to the brain surface. As for rats, electrode was removed, incision closed, anesthetic/antibiotic applied, and mice monitored prior to returning to home cages.

Administration of Minocycline

Postinjury immune response was blunted using the tricyclic antibiotic minocycline. Selected rats received two acute minocycline doses (Sigma-Aldrich, Co., St. Louis, MO) of 45 mg/kg i.p., administered at 30 min and 6 h after UEC, a paradigm previously shown to induce immunosuppression (Homsi et al., 2009). Control animals underwent the same procedure but received saline vehicle.

Protein Extraction

Selected animals were anaesthetized with 4% isoflurane in carrier gas of 70% N_2O, 30% O_2 for 4 min, then sacrificed by decapitation at 1, 2, 4, or 7d after UEC, with whole hippocampus and molecular layer (ML) dissected (n=4/group) for assessment of protein expression. In the minocycline experiments, rats were sacrificed at 2d postinjury and hippocampi dissected (n=4 each saline and minocycline treated). Tissue samples were homogenized on ice in 125 μl of T-PER (Thermo Scientific, Rockford, IL), and centrifuged at 8,000 × g for 5 min at 4°C. Supernatant was aliquoted and stored at −80°C. Prior to Western blot (WB), or zymography analysis, protein concentration was determined using Thermo Scientific Pierce Protein Assay Reagent (Rockford, IL) and the FLUOstar Optima plate reader (BMG Labtech, Inc., Durham, NC).

Western Blot

WB analysis was carried out utilizing Bio-Rad products (Hercules, CA). Twenty μg of protein were prepared for WB with XT sample buffer and reducing buffer, then denatured. Samples were electrophoresed on 4–12% Bis-Tris Criterion XT gels (200 V × 45 min) and protein transferred to polyvinylidene fluoride (PVDF) membranes. Post-blot gels were stained with 0.1% coomassie brilliant blue (40% methanol (MeOH), 10% glacial acetic acid), then destained at RT to confirm even transfer. To prevent non-specific binding, membranes were blocked in 5% milk Tris-Buffered Saline with 0.05% Tween 20 (mTBST). Blots were then incubated overnight at 4°C in mTBST with individual primary antibodies (goat anti-OPN 1:200, R&D Systems, Minneapolis, MN; rabbit anti-OPN 1:500, Rockland Immunochemicals Inc., Gilbertsville, PA; rabbit anti-MAP1b 1:200, Santa Cruz Biotechnology, Dallas, TX; mouse anti-N-cadherin 1:1000, B D Transduction Labs, San Jose, CA; goat anti-synapsin-1a/b 1:200, Santa Cruz Biotechnology, Inc., Dallas, TX; rabbit anti-LCN2 1:200, Santa Cruz Biotechnology, Inc., Dallas, TX). The region of each blot below 25kD was probed with rabbit anti-cyclophilin A (1:2,500, Millipore, Billerica, MA) as loading control. Blots were next washed with mTBST and incubated with appropriate

secondary in mTBST (1:10,000 goat anti-mouse, Rockland Immunochemicals, Gilbertsville, PA; 1:20,000 bovine anti-rabbit, 1:20,000 bovine anti-goat Santa Cruz Biotechnology Inc., Dallas, TX) at RT for 1 h. Finally, blots were TBST washed and incubated with Super Signal Dura West chemiluminescent substrate (Thermo Scientific, Rockford, IL) for signal detection. WB images were captured with Syngene G:Box and positive band signal subjected to densitometric analysis (relative optical density, ROD) with Gene Tools software (Syngene, Frederick, MD). Protein data were expressed as either fold change over controls or percent change relative to paired control cases run on same blot membrane.

Gelatin Zymography

Twenty μg of protein from 2d hippocampal extracts described above were prepared with 2x Tris-glycine SDS sample buffer then separated by gelatin electrophoresis at 4°C on Novex® 10% zymogram gels (Life Technologies, Grand Island, NY). Gels were renatured in Novex® Zymogram Renaturing Buffer (Life Technologies, Grand Island, NY) at RT before development in Novex® Zymogram Developing Buffer over 6 d at 37°C. Gelatin lysis was visualized with coomassie brilliant blue and purified enzyme run as positive control. Zymogram signal was inverted and captured on Syngene G:Box, and densitometry analyzed as ROD with Gene Tools software (Syngene, Frederick, MD). Enzyme activity was expressed as percent change relative to paired controls run on the same gel.

Immunohistochemistry

At 1 and 2d after UEC (n=4/group), rats were prepared for fluorescent immunohistochemical (IHC) analysis according to published protocol (Warren et al., 2012). Animals were anaesthetized with sodium pentobarbital (90 mg/kg, i.p.), transcardially perfused with 0.9% saline followed by 4% paraformaldehyde in 0.1M $NaHPO_4$, pH=7.4, after which brains were extracted and placed in fixative for 24 h before transfer to 0.03% NaN_3 in 1.0 M phosphate buffered saline (PBS). For IHC, brains were blocked at the dentate gyrus and 40 μm coronal sections were sliced using the VT1000S microtome (Leica, Buffalo Grove, IL). To prevent non-specific binding, sections were blocked in Blotto (5% Cold Water Fish Skin Gelatin, Aurion, Netherlands, 0.5% Triton in 1.0 M PBS) for 30 min prior to overnight incubation with Blotto containing primary antibody (mouse anti-OPN MPIIIB10 1:300, Iowa Hybridoma, Iowa City, IA; rabbit anti-IBA1 1:300, Wako Chemicals, Richmond, VA; rabbit anti-GFAP 1:20,000, Dako, Carpinteria, CA; goat anti-synapsin-1a/b 1:250, Santa Cruz Biotechnology, Inc., Dallas, TX). The next day, free floating tissue sections were washed with PBS, blocked in Blotto at RT, then incubated with the appropriate secondary antibody (Alexa Fluor® 488 or 594, 1:1,000, Life Technologies, Grand Island, NY) in Blotto for 1 h at RT. Sections were then PBS washed, equilibrated in phosphate buffer, and mounted on Superfrost Plus slides (Fisher Scientific, Pittsburgh, PA) with Vectashield (Vector Laboratories, Burlingame, CA). IHC signal was visualized on the TCS-SP2 AOBS (Leica, Buffalo Grove, IL) or LSM 700 (Carl Zeiss, Thornwood, NY) confocal microscope.

qRT-PCR

At 1 or 2d after UEC, selected rats were anesthetized, decapitated, and whole hippocampi or ML fractions dissected (n=10/group). Total RNA was extracted with TRIzol® (Life

Technologies, Grand Island, NY) then processed for OPN gene assessment utilizing Qc analysis and qRT-PCR with TaqMan® Assay Reagents (Life Technologies, Grand Island, NY). Probes and primer sets for detection of OPN (Rn00582114m1) were obtained from Inventoried Assays (Life Technologies, Grand Island, NY). Probes were labeled at the 5' end with 6-carboxyfluorescein and with a dark quencher at the 3' end. Efficiency was determined with 10-fold serial dilutions of template and cyclophilin A was used as an endogenous control (Pre-developed TaqMan® Assay Reagents; Life Technologies, Grand Island, NY). Experiments were performed in the ABI Prism 7500 Sequence Detection System using the TaqMan® One-Step PCR Master Mix Reagents Kit (Life Technologies, Grand Island, NY). Samples were tested in triplicate under cycling conditions (48°C/30min, 95°C/10 min; 40 cycles 95°C/15 sec, and 60°C/1 min). Fold change in OPN mRNA was calculated by the $2^{-\Delta\Delta Ct}$ method (Dumur et al., 2009).

In Situ Hybridization

Sense and antisense probes were generated against full length OPN (Spp1, MRN1768-202780755) and synaptobrevin (Vamp1, MRN1768-202782932), the latter used as a positive control (Thermo Scientific, Rockford, IL). Riboprobes were synthesized using digoxigenin (DIG)-tagged dNTPs (Roche, Mannheim, Germany) and the MAXIscript® in Vitro Transcription Kit (Life Technologies, Grand Island, NY), after which they were hydrolyzed to ~500nt as previously described (Su et al., 2010). Selected 40 μm coronal sections from 2d postinjury animals and controls (n=3/group) used for IHC studies were again mounted on Superfrost Plus slides (Fisher Scientific, Pittsburgh, PA), then hybridized at 65°C as previously described (Yamagata et al., 2002). Bound riboprobes were detected by horseradish peroxidase (POD)-conjugated anti-DIG and fluorescent Cy3 staining with Tyramide Signal Amplification (TSA) systems (PerkinElmer, Shelton, CT). For fluorescent ISH and antibody co-labeling, standard IHC was performed following the TSA step. ISH/IHC signal was visualized using the TCS-SP2 AOBS (Leica, Buffalo Grove, IL) confocal microscope.

Genotype Confirmation and Protein Ablation Verification for KO Mice

Confirmation of transgenic OPN KO was assessed utilizing the PCR-verification method of the Jackson laboratory to test for presence of the neo^rcassette replacing exons 4–7 of the OPN gene, responsible for creating a null mutation, and rendering the animal incapable of producing an OPN transcript in B6.129S6 (Cg)-*Spp1*^{tm1Blh}/J mice (Liaw et al., 1998). Genomic DNA was isolated from 1cm of tail snips, and genotyping confirmed utilizing the oIMR8444 primer '5GCC TGA AGA ACG AGA TCA GC3' for OPN and HotSHOT method (Truett et al., 2000; Su et al., 2010). To confirm the absence of OPN gene product in these animals, protein expression in the injured hippocampus was assessed. OPN KO and WT hippocampal protein extracts from mice subjected to UEC were analyzed by WB as described above, using goat anti-OPN (0.25 μg/ml, R&D Systems, Minneapolis, MN).

Novel Object Recognition

Cognitive performance was assessed using a modified novel object recognition (NOR) test based on previous studies (Ennaceur and Delacour, 1988; Han et al., 2011; Baratz et al.,

2011; Siopi et al., 2012). The NOR apparatus consists of a 42 × 42 × 30 cm^3 open field arena under red light illumination (1 lux at mouse height) in a sound-isolated room (Fuller et al., 2012). The NOR task consists of three phases: habituation, familiarization, and testing. During habituation (3, 6, 13, 20, 27d postinjury), UEC (C57BL/6 n=12, OPN KO n=9) or uninjured (C57BL/6 n=12, OPN KO n=12) mice were acquainted with the black opaque plastic testing chamber for two nonconsecutive 5 min intervals. Twenty four hours later, animals started the familiarization phase in the same chamber and were allowed to explore two identical objects: 50-mL conical plastic tubes affixed to the floor with Velcro® tape in symmetrical positions within the chamber. After a 1h delay, the animals entered the testing phase (4, 7, 14, 21, 28d postinjury) and returned to the chamber where one of the objects was replaced by a new object: a Lego® DUPLO® configuration of similar material and dimensions (h × w), but differing in shape from that of the conical tube. Time spent exploring each object during both the familiarization and testing phases was recorded at one min periods with an overhead video camera, and later scored. Object exploration was operationally defined as object touching, or orienting behaviors (sniffing, rearing, or head orientation) occurring within 2 cm of the object. Sitting on top of or circling was not counted. To prevent olfaction distraction or bias, the chamber and objects were thoroughly cleaned with 70% ethanol between trials. To avoid confounding effects of long term memory, a different novel object configuration was presented during each progressive trial. Results of the testing phase are represented by recognition index (RI=time spent with novel object/(time spent with familiar object+time spent with novel object) × 100). RI score of 50 represents a chance level of performance (no object preference) and RI significantly greater than 50 indicates an intact memory capacity for this task. Similar to previous reports (Meunier et al., 2013); a small percentage of mice did not explore either object, but engaged in unrelated behaviors (e.g., grooming or freezing). As determined with these earlier studies, no RI can be calculated from such behavior and mice which exhibited the non explorer pattern for greater than 50% of the recorded time (n=2 WT and n=5 OPN KO) were excluded prior to data analysis.

Statistical Analyses

Changes in rat protein or RNA levels, due to injury or minocycline treatment, were evaluated using the General Linear Model (GLM) in SPSS v.11. The time course of changes in OPN protein and transcript after UEC injury was assessed using a mixed model analysis of variance (ANOVA) with hemisphere (contralateral vs. ipsilateral to injury) as a within-subjects variable, and day postinjury as a between-subjects measure. The significance of changes at specific postinjury days was evaluated as *a priori* planned comparisons using simple-main effects based on marginal means, and implemented using multivariate ANOVA (MANOVA) routines in SPSS.

For the mice studies, changes in protein levels or enzyme activity, induced by injury or associated with genetic strain, were evaluated using GLM in SPSS v.11. These alterations were assessed using a mixed model ANOVA with hemisphere (contralateral vs. ipsilateral to injury) as a within-subjects variable, and strain as a between-subjects measure, and specific pairwise comparisons evaluated as simple main effects. The effects of strain and UEC injury on NOR behavioral performance, was evaluated with a completely randomized ANOVA

design followed by Duncan post-hoc tests. Both rat and mouse results are reported as mean +/− SEM. An alpha level of 0.05 was used in all analyses.

Results

Osteopontin Expression Is Time Dependent Following UEC

We first examined the postinjury time course of OPN protein expression during UEC adaptive synaptogenesis, focusing on acute survival intervals of initial immune response (1d) and onset of presynaptic degeneration (2d). These time points were contrasted with the pre-regenerative interval (4d) and a time point matching onset of presynaptic terminal sprouting (7d). In hippocampal extracts we performed routine WB using an OPN antibody (R&D Systems) which identified full length OPN (66 kD) as the principal signal, with low affinity for OPN fragments. In contralateral control hippocampi, signal was detected, but close to background, supporting the reported low constitutive expression of full length OPN in brain (Choi et al., 2004; Iczkiewicz et al., 2004). In the deafferented hippocampi, results showed a significant time-dependent change in full length 66 kD OPN protein ($F_{(3,12)}$=54.94; p<0.001), with increases initiated by 1d (29.4 ± 1.4 fold, p<0.001), peaking at 2d (51.6 ± 2.6 fold, p<0.001), and no longer significantly different from control level at 4d (3.4 ± 0.5 fold, p=0.522) (Fig. 1A). At the 7d onset of sprouting, OPN protein returned to control level (1.2 ± 0.2 fold, p=0.955). Given these WB results, hippocampal tissue sections were subjected to OPN IHC at 1 and 2d postinjury, probing for change in protein distribution within the deafferented ML. Here we applied a second OPN antibody (Iowa Hybridoma) raised against bone protein fractions which is used to identify OPN in situ. Interestingly, OPN signal was present within granule cell bodies of the dentate gyrus (Fig. 1B), with a diffuse, low level label over the dentate ML. At 1d following UEC, only modest differences in OPN staining were observed between injured and control ML, however, at 2d there was a prominent increase over the deafferented zone, appearing as both punctate and cellular labeling, consistent with OPN localization around and within reactive glia. Granule cell OPN signal did not show remarkable change at either postinjury interval. This acute increase in full length OPN 1–2d after UEC matches that reported for other models of CNS trauma (Ellison et al., 1998; Hashimoto et al., 2003; Shin et al., 2005), where onset of OPN elevation occurs within 24 hours after injury. Focal elevation of OPN over regions of synaptic reorganization is also consistent with the fact that MMP-3, one matrix enzyme which cleaves OPN to expose integrin binding epitopes, shows similar spatial and temporal increase after UEC (Falo et al., 2006).

Since OPN proteolytic fragments can potentially signal glial reactivity, we utilized a third OPN antibody (Rockland) that recognizes a 32 kD MMP-cleaved OPN fragment, probing for potential MMP processing on the lesioned side. In extracts of the deafferented dentate, 32 kD OPN expression was significantly altered relative to control ($F_{(1,8)}$=8.05; p<0.05). Analyses at specific postinjury days revealed 1d elevation of the 32 kD band (128.8 ± 12.4%, p<0.05), which was no longer different from controls at 2d. We also observed an intermediate OPN fragment, migrating at approximately 48kD, which was significantly altered after UEC ($F_{(1,8)}$=12.83; p<0.01). At 1d postinjury, its expression was similarly increased over controls (166.2 ± 24.1%, p<0.01). This higher kD band is detected by the

Rockland antibody after in vitro MMP lysis of purified OPN, and may result from MMP cleavage at C-terminal loci downstream of the Rockland antigenic site (Scatena et al., 2007). Together, these observations suggest that OPN contributes to acute cell-mediated immune response after deafferentation, and supports a role for OPN in reactive synaptogenesis.

Reactive Glia Express Osteopontin During Synaptogenesis

To determine the identity of OPN labeled cells within the deafferented ML, we performed IHC double label co-localization of OPN with antibodies specific for microglia (IBA1) and astrocytes (GFAP). After UEC, increased OPN staining in the deafferented zone was associated with reactive microglia and astrocytes (Fig. 2), where a low level of OPN signal was seen in paired contralateral controls. Overall, OPN in the deafferented ML increased between 1 and 2d postinjury, with microglia exhibiting greater labeling. A subset of reactive microglia was found along the boundary of outer deafferented dendrites and the inner non-deafferented ML, marking the interface between intact and damaged synapses. Such alignment was present but not as striking for OPN positive astrocytes. These results suggest that acute OPN increase during deafferentation-induced synaptogenesis is principally glial in nature, and that early OPN role may be mediated through inflammation and reactive microglia. Similar OPN localization within reactive glia was reported for CNS cortical injury (Shin et al., 2005; von Gertten et al., 2005; Plantman, 2012), and following both stroke and ischemia (Ellison et al., 1998; Choi et al., 2007). Prior UEC studies also show that activated microglia position themselves along dendritic boundaries. At these sites they have the potential to interact with matrix proteins such as agrin to direct synaptic reconstruction (Falo et al., 2008), and secrete MMP-3 (Falo et al., 2006), providing a glial pathway for generating OPN/integrin signals.

Osteopontin Transcript Elevated in Microglia of Deafferented Zone

Given that OPN protein was significantly elevated during the acute phase of reactive synaptogenesis, and that this elevation was largely cellular in the ML, we applied qRT-PCR and ISH to assay OPN transcription. Preliminary microarray screening revealed a 13.6 fold increase in whole hippocampal OPN mRNA with UEC, while the deafferented ML showed a 21.1 fold elevation. We performed qRT-PCR on RNA extracts from either whole hippocampi or dentate ML at 1 and 2d after UEC lesion. Results showed multifold elevations of OPN mRNA, which were highly significant for both whole hippocampus ($F_{(1,7)}$=192.30; p<0.001) and ML ($F_{(1,6)}$=50.82; p<0.001) relative to levels in paired contralateral control hemispheres (Fig. 3A). Significant injury-induced elevation of hippocampal OPN transcript was seen at each time point (75.0 ± 23.3 fold for 1d; 79.3 ± 31.1 fold for 2d; p<0.001). ML extracts showed an even greater magnitude of change in OPN transcript compared with control levels (126.6 ± 55.7 fold for 1d; 150.1 ± 44.2 fold for 2d, p<0.001). When 2d postinjury UEC cases were subjected to ISH with digoxigenin (DIG)-tagged riboprobe for OPN transcript (Su et al., 2010), antisense binding was localized within IBA1 positive reactive microglia of the deafferented zone (Fig. 3B). Parallel post hybridization sections were stained with GFAP antibody and no mRNA signal was observed in ML reactive astrocytes (Fig. 3C). Sense control binding was negative (Fig. 3D), confirming signal specificity. These results suggest reactive microglia as a principal source

of OPN production within deafferented ML during the acute phases of reactive synaptogenesis.

Immunosuppression Alters OPN Response and Terminal Degeneration Following UEC

Collectively, the present data support induction of an acute OPN response with deafferentation, likely through microglial activation to facilitate early stages of synaptic reorganization. Since OPN is elevated under conditions of inflammation (Patarca et al., 1989; Hwang et al., 1994; Weber and Cantor, 1996; Chabas et al., 2001), and can direct the migration of macrophages and microglia to sites of brain injury (Ellison et al., 1998; Shin et al., 2011; Hashimoto et al., 2003), it is possible that manipulation of inflammation will affect OPN role in these processes during early synaptogenesis. To test this possibility, we used the tricyclic antibiotic minocycline (delivered acutely at 30 min and 6 h post-UEC lesion) to attenuate inflammatory response, as well as reduce microglial activation (Yrjanheikki et al., 1998; Yrjanheikki et al., 1999). We then examined the effect of minocycline on hippocampal OPN expression by WB, and found that the drug significantly attenuated injury-induced elevation of full length OPN at 2d postinjury by about 53% ($F_{(1,6)}$=77.83; p<0.001), from 48.6 fold to 22.6 fold. Next, we assessed whether the antibiotic affected OPN lysis, utilizing gelatin zymography and WB to evaluate MMP activity and the presence of OPN fragments, respectively. Consistent with prior studies documenting increased MMP activity during the acute postinjury debris clearance (Kim et al., 2005; Falo et al., 2006), we observed significant elevations in the activity of hippocampal MMP-2 ($F_{(1,4)}$=260.39; p<0.001) and MMP-9 ($F_{(1,4)}$=14.55; p<0.05) at 2d following UEC (Fig 4A). Acute administration of minocycline did not alter injury-induced MMP-2 activity relative to the control hemisphere (374.1 ± 34.0% in vehicle versus 351.8 ± 39.5% in treated), but significantly reduced MMP-9 proteolysis by more than 41% ($F_{(1,4)}$=23.19; p<0.01), from 370.4 ± 35.5% to 152.5 ± 28.1% (Fig. 4A). This result is consistent with minocycline inhibition of MMPs in models of CNS trauma and stroke (Machado et al., 2006; Cayabyab et al., 2013). We also evaluated the effect of minocycline on MMP-generated OPN fragments, using the Rockland antibody to probe for differences in their generation compared with saline-treated controls at 2d postinjury (Fig. 4B). Minocycline treatment did not alter 32 kD OPN fragment expression ($F_{(1,6)}$=1.07; p=0.340), however, injury-induced elevation of the 48 kD OPN signal (123.1 ± 15.4%) was significantly reduced by 54% after drug treatment to 56.7 ± 16.0% ($F_{(1,5)}$=8.66; p<0.05). These observations suggest that postinjury MMP-9/OPN interaction contributes to the generation of OPN fragments with exposed integrin binding sequences. Such integrin-mediated signals could promote removal of debris and degenerating terminals in the early stages of synaptic repair.

In order to document cellular distribution of OPN with minocycline treatment, we performed double label IHC with OPN and the microglial marker IBA1 (Fig. 5). Results suggested that OPN positive microglia were more randomly distributed after minocycline. This cellular change was tested for correlation with extent of presynaptic terminal removal during the early phases of reactive synaptogenesis. Notably, minocycline effect on microglia was associated with abnormal presynaptic terminal loss at 2d after UEC (Fig. 5). Vehicle treated animals show predicted clear loss of presynaptic marker synapsin-1 over deafferented ML

(Lund and Lund, 1971; Greif and Trenchard, 1988); however, minocycline treatment resulted in an altered synapsin-1 distribution. Synapsin-1 signal at the inner/outer ML zone boundary was less crisp and the presynaptic terminal marker mapped a diffuse, irregular pattern, extending into the deafferented neuropil. Together, these results suggest that partial inhibition of OPN is correlated in space and time with altered pre-synaptic terminal loss and microglial response, likely attenuating the critical early degenerative phase of reactive synaptogenesis.

Osteopontin Knockout Differentially Affects Markers of Synaptic Reorganization After UEC

In order to specifically test OPN role during reorganization of synaptic structure, we generated UEC lesions in homozygous OPN KO mice (Liaw et al., 1998) and examined whether the loss of OPN affected expression of molecular markers of dendritic, synaptic and axonal plasticity. First we confirmed genotype of these mice by performing PCR-verification according to published protocol (The Jackson Laboratory), and verifying the presence of the neo^{r}cassette replacing OPN exons 4–7, which creates a null mutation, rendering the gene incapable of producing functional OPN protein in B6.129S6(Cg)-*Spp1*^{tm1Blh}/J mice (Fig. 6A). In addition, we showed that 2d postinjury elevation in OPN protein observed for rat samples was reproduced in WT mice subjected to UEC, an effect ablated with OPN KO. WT C57BL/6 mice showed robust increase in hippocampal OPN compared to contralateral controls (88.38 ± 0.67 fold, $p<0.001$). This was in contrast to a null OPN response ipsilateral to lesion for OPN KOs, whose blot signal was no longer detectable above background. These data confirmed knockout of the OPN gene and protein for our population.

Next we explored the relationship between OPN and dendritic cytoskeletal reorganization during synaptogenesis, using microtubule associated protein (MAP) as a surrogate marker. Given that intracellular OPN interacts with the cytoskeleton through MAP1B binding (Long et al., 2012), we investigated the potential for OPN to affect postinjury reshaping of dendritic structure by looking for differences in MAP1B expression between OPN KO and WT animals subjected to UEC. Here we utilized WB methods to assess 2d hippocampal MAP1B expression, detecting three principal bands at 220, 80, and 35 kD (Fig. 6B). The 220 kD signal reflects full length MAP1B, while 80 and 35 kD represent fragments generated by calpain- or caspase-mediated cleavage, pathways important for cytoskeletal reorganization after neural injury (Fifre et al., 2006). Results showed an overall significant decrease within the deafferented hippocampus in the 80 kD band ($F_{(1,5)}=151.28$; $p<0.001$), while UEC-induced changes were not significant for the 220 kD ($F_{(1,5)}=5.15$; $p=0.073$) or the 35 kD ($F_{(1,5)}=0.977$; $p=0.368$) bands. Notably, no significant difference in MAP1B expression was detected between the two mouse strains. In WT, MAP1B levels were significantly lower for the 80 kD fragment (51.6 ± 3.1%, $p<0.001$), whereas decreases in the 220 kD full length form (76.9 ±10.7%, $p=0.251$) and the 35 kD fragment (91.2 ± 2.9%, $p=0.079$) did not reach significance. For OPN KO mice, hippocampi showed changes similar to those of WT MAP1B, with a significant decrease in the 80 kD form (46.8 ± 7.1%, $p<0.001$), and no significant changes for 220 kD (82.9 ± 10.7%, $p=0.106$) and 35 kD (104.1 ± 8.0%, $p=0.574$). While WB data fail to identify WT and OPN KO differences in MAP1B expression, significant reduction of 80 kD MAP1B within both strains suggests processing

of MAP1B plays an important role during cytoskeletal reorganization in the deafferented mouse model.

In a second experiment, we examined WT and OPN KO changes in N-cadherin expression after UEC, utilizing the molecule as a marker of acute synapse destabilization and morphing. N-cadherin, a transmembrane adhesion protein exhibits homologous binding to stabilize the synaptic junction. Hippocampal N-cadherin protein was assessed using WB analysis, again focusing on 2d postinjury, matching the interval of maximal OPN response previously shown in the rat model (Fig. 6C). Here we evaluated full length 115 kD N-cadherin, and a 35 kD cleaved fragment. In the deafferented hemisphere, we observed a significant overall decrease in the 115 kD band ($F_{(1,6)}$=37.26; p<0.001), suggesting that N-cadherin breakdown was correlated with synapse destabilization during acute degeneration. As with MAP1B, no strain differences were detected. Relative to contralateral controls, injured WT hippocampi had lower expression of both 115 and 35 kD N-cadherin (73.9 ± 2.1%, p<0.01; 73.2 ± 14.5%, p=0.168), however, only the full length reached significance. For OPN KOs, 115 kD N-cadherin level was significantly reduced (82.9 ±5.7%; p<0.05), and the 35 kD fragment was highly variable, not different from control levels (105.2 ± 25.4%; p=0.535). Since N-cadherin localizes within ML reactive astrocytes after UEC (Warren et al., 2012), these results are consistent with the hypothesis that reactive glia can mediate the proteolysis of full length N-cadherin to facilitate synaptic reshaping during reactive synaptogenesis.

As a third approach, we used synaptic vesicle protein synapsin-1 to explore the effect of OPN loss on extent of presynaptic terminal degradation during acute degenerative phase of synaptogenesis. Given the correlation between OPN reduction and degree of synapsin-1 clearance in UEC rats treated with minocycline, we predicted that WB profile of hippocampal synapsin-1 expression in WT and OPN KO mice would differ after UEC. As assessed at 2d postinjury, UEC induced highly significant overall decreases in full length 80 kD synapsin-1 ($F_{(1,5)}$=60.69; p<0.001), and in a cysteine protease-cleaved 55 kD product ($F_{(1,5)}$=146.41; p<0.001) (Fig. 6D). Assessments of full length synapsin-1 showed similar reductions in the deafferented hemisphere for WT (66.6 ± 5.4%; p<0.01) and KO (73.6 ± 1.4%, p<0.01). Like MAP1B and N-cadherin, a reduction would be predicted given the overall proteolysis occurring in the deafferented zone. However, in contrast to MAP1B and N-cadherin, analysis of the 55kD synapsin-1 cleavage fragment showed a significantly greater decrease in WT (52.6 ± 4.7%; p<0.001) than in KO (83.2 ± 3.6%; p<0.05) ($F_{(1,5)}$=23.20; p<0.01). With OPN KO, breakdown of this synapsin-1 fragment was approximately 30% less than in WT animals, a result consistent with the incomplete removal of synapsin-1 in the rat UEC model when OPN expression was attenuated by minocycline. In order to confirm altered synapsin-1 processing in vivo, we used IHC to document synapsin-1 distribution in OPN KO animals. Here we observed immunobinding differences between WT and KO strains at 2d after UEC (Fig. 7). In WT cases the deafferented outer ML synapsin-1 labeling was notably reduced, reflecting early removal of degenerating presynaptic terminals (Fig. 7B). By contrast, in OPNKO animals, significant synapsin-1 signal remained over the middle ML, consistent with abnormal synaptic reorganization during this early phase of reactive synaptogenesis (Fig. 7D). Collectively, these results suggest that loss of OPN impairs removal of degenerating presynaptic terminals.

Lipocalin 2 Regulation of UEC-Induced MMP-9 Activity Changes With Osteopontin Knockout

Given that MMP-9 activity and production of OPN fragments with integrin signaling properties were correlated after rat UEC, we wanted to determine the extent to which injury-induced MMP-9 activation would be altered under conditions of OPN KO. It was hypothesized that if OPN is a principal substrate of MMP-9 in the deafferented hippocampus, then loss of OPN would attenuate both the enzyme activity and potential MMP-9 regulatory molecules. The secreted siderocalin LCN2 binds and persistently activates MMP-9 (Tschesche et al., 2001), offering an ECM mechanism for MMP-9 regulation after UEC. To test this possibility we used zymography to assay MMP-9 activity and WB to measure LCN2 expression in OPN KO mice subjected to UEC. As for the rat model, we found UEC to induce significant overall increases in MMP-2 ($F_{(1,7)}$=43.53; p<0.001) and MMP-9 ($F_{(1,6)}$=78.82; p<0.001) activity (Fig. 8A). Activity increases in MMP-2 were not significantly different between WT (248.2 ± 31.6%, p<0.01) and KO (215.6 ± 36.0%, p<0.01) mice. However, elevation of MMP-9 activity in the deafferented hemisphere of WT (1385.3 ± 196.2%, p<0.001) was significantly greater than that observed in KO mice (650.4 ± 215.5%, p<0.01) ($F_{(1,6)}$=6.36; p<0.05). In parallel LCN2 WB experiments, we found UEC to induce overall significant increases in the predicted 130 kD MMP-9 bound form (Park et al., 2009) ($F_{(1,6)}$=2604; p<0.01) and a second 55 kD band ($F_{(1,6)}$=203.09; p<0.001) (Fig. 8B). UEC induced significant LCN2 increases in WT (775.99 + 170.4%, p<0.01), whereas the LCN2 elevation in the deafferented hemisphere of KO mice (271.8 + 54.1%; p=0.075) was not significantly different from the control hemisphere. This strain difference in LCN2 level was significant ($F_{(1,6)}$=7.95; p<0.05). Regarding the 55 kD LCN2 band, UEC resulted in significant increases for both WT (237 + 17.7%; p<0.001) and KO (183.4 + 13.5%; p<0.001), although these changes narrowly missed demonstrating a significant difference between the two strains ($F_{(1,6)}$=5.92; p=0.051). While correlative, and limited to one regulatory mechanism, these results suggest that part of UEC-induced MMP-9 activity may be mediated by LCN2 binding, and that enzyme activity is associated with the presence of OPN.

Absence of Osteopontin Impairs Recovery of Cognitive Function Following UEC

Given that UEC induced hippocampal synaptogenesis in the rat is temporally correlated with recovery of cognitive function (Steward, 1998), and that our aggregate data support a role for OPN during the initial phases of synaptic reorganization after brain injury, we tested whether cognitive function was affected when OPN KO mice were subjected to UEC. The NOR task was utilized to examine hippocampal-dependent long term memory function (Fig. 9). Naïve WT and OPN KO mice were initially evaluated to confirm no behavioral task differences between strains. Both uninjured WT and OPN KO animals successfully recalled the familiar object, spending significantly more time exploring the novel object compared to chance alone (68.5 ± 1.6%, p<0.001; 65.2 ± 4.1%, p<0.01). Following UEC, mice were evaluated over a 28d postinjury window, inclusive of the early collateral sprouting (4d) and synapse reformation (7d) phases, as well as once a week (14, 21, 28d) during the synapse maturation and stabilization phases. Interestingly, WT mice successfully recalled the familiar object after UEC, having RI values significantly above chance throughout the entire testing period. With UEC, it is possible that WT RI remained above criterion due to

compensation of intact contralateral hippocampal circuitry. While WT performed similar to naïve mice at 4d (68.5 ± 2.4%, $p<0.001$), their RI values did decline throughout the subsequent sprouting and maturation periods: 7d (65.3 ± 2.9%, $p<0.001$), 14d (62.4 ± 2.8%, $p<0.01$), and 21d postinjury (57.8 ± 2.9%, $p<0.05$). By 28 d WT RI scores were again equivalent to those of uninjured mice (66.4 ± 1.9%, $p<0.001$), perhaps due to long term strengthening of synaptic connections. This time dependent reduction and rebound in NOR performance is similar to that reported for the same WT strain subjected to concussive TBI (Han et al., 2011). For the OPN KO group, animals did meet criterion for recognizing the familiar object at 4d (57.1 ± 3.4%, $p<0.05$), however, RIs were significantly lower than WT mice ($p<0.05$). Notably, OPN KO animals failed to reach task criterion at 7d (55.9 ± 7.0%; $p=0.393$), 14d (59.1 ± 6.1%; $p=0.323$), and 21d (60.1 ± 4.2%; $p=0.082$), with highly variable exploratory behavior. Nevertheless, OPN KO behavior did improve over the testing period, mice spending more time with the novel object between days 14 and 28. Like WT, OPN KO behavioral performance was consistent with time-dependent circuit restoration, achieving RI values above criterion at 28d (62.6 ± 4.6%, $p<0.01$). Overall, WT mice subjected to UEC performed better than OPN KOs and, while OPN loss did not prevent NOR recovery, the absence of OPN impaired the time course of that recovery.

Discussion

This study examined time dependent OPN expression following hippocampal deafferentation. OPN protein rose approximately 50 fold 1–2d postinjury with adaptive synaptic plasticity, a change mapped to activated glia of the deafferented zone. OPN transcript increased over 50 fold, and was localized within microglia, a subset of which aligns along the deafferented zone boundary. Minocycline immunosuppression attenuated MMP-9 gelatinase activity and 48kD OPN fragment generation. The antibiotic also affected removal of synapsin-1 positive degenerated axons. UEC in OPN KOs similarly reduced hippocampal MMP-9 activity and synapsin-1 breakdown, but MAP1B and N-cadherin, cytoarchitecture and synaptic adhesion surrogates, were not affected. Parallel IHC for synapsin-1 in OPN KO animals suggests attenuation of degenerating presynaptic terminal removal over the deafferented zone. Loss of OPN also decreased MMP-9 activity, concurrent with reduced expression of a predicted LCN2 bound form. OPN KOs subjected to UEC exhibited time dependent cognitive deficits during synaptogenesis. These results support the hypothesis that OPN signals glial migration and removal of degenerated axons, preparing deafferented sites for restored functional input.

OPN protein and mRNA expression was temporally correlated with cellular processes directing adaptive synaptogenesis. OPN increased robustly 24 h postinjury, tracking acute inflammation. Its rapid elevation occurs following toxic insult (Morita et al., 2008), stroke (Wang et al., 1998), ischemia (Lee et al., 1999; van Velthoven et al., 2011) and spinal cord injury (SCI) (Hashimoto et al., 2003; Moon et al., 2004). OPN normalization by 7d points to an inflammatory role supporting acute degeneration. Other cytokines also increase after human TBI (Helmy et al., 2011), and with rodent impact acceleration (Shohami et al., 1994), fluid percussion (Vitarbo et al., 2004), cortical impact (Kelso et al., 2011), and blast neurotrauma (Dalle Lucca et al., 2012). While TBI OPN studies are limited, OPN rise with inflammation after cortical impact (von Gertten et al., 2005; Israelsson et al., 2006),

cryolesion (Shin et al., 2005), and stab wound (Plantman, 2012) are documented. Our study is the first to map OPN during trauma-induced synaptogenesis, providing evidence for acute MMP cleavage of OPN into fragments with potential to signal glial mobilization and tissue reorganization. OPN and integrin receptor interaction after facial nerve axotomy (Kloss et al., 1999), potentially mediates growth factor directed regeneration (Cunningham et al., 2005; Lu et al., 2008). Similar OPN control of cell activation, mobility and regeneration was postulated after hemorrhagic lesion (Ellison et al., 1998), cryolesion (Shin et al., 2005), and stab wound (Plantman, 2012). The present results are consistent with integrin receptor up-regulation during postinjury reemergence of long term potentiation (LTP), a functional correlate of synaptogenesis (Milner and Campbell, 2002; Nikonenko et al., 2003). Acute OPN increase within reactive neuroglia of deafferented hippocampus is consistent with its rapid elevation in tissue extracts. OPN transcript was also detected at 1d in reactive microglia, but not astrocytes, similar to its localization 24h after stroke (Ellison et al., 1998). Notably, the latter study also found 15d OPN mRNA increase within astrocytes at repair onset. Delayed astrocyte OPN expression was also reported after SCI (Hashimoto et al., 2003) and ischemia (Choi et al., 2007).

In light of acute OPN fragment rise after UEC, we posit that OPN contributes to glial paracrine signaling during evolution of TBI synaptic plasticity. OPN could influence postinjury glia several ways. It binds MAP1A and MAP1B (Long et al., 2012), affecting cytoskeletal stabilization-destabilization. However, this seems less likely after UEC since IHC revealed little OPN/MAP1B co-localization (*data not shown*). More plausible is OPN activation/mobilization of neuroglia to direct successful synaptic repair, as proposed in the cellular model presented in Fig. 10. With the activation of local glia, dying axon terminals can be removed and regenerative terminal sprouting induced (Steward, 1989; Sofroniew, 2000; Belanger and Magistretti, 2009; Hamby and Sofroniew, 2010). MMPs secreted by reactive glia generate local OPN fragments, capable of directing degenerative/regenerative shifts during synaptic repair (John et al., 2003; Pellerin and Magistretti, 2004). Increased LCN2 binding/activation of MMP9 likely contributes to this process. OPN fragments can also stimulate microglial activation, shifting the cells into a pro-inflammatory M1 state, as well as induce macrophage proliferation to facilitate phagocytosis (Tambuyzer et al., 2012). OPN producing macrophages participate in debris clearance after stroke (Shin et al., 2011) and CNS demyelination (Zhao et al., 2008). Acutely, OPN can stimulate reactivity of astrocytes at sites of deafferentation, enhancing MMP targeting of ECM proteins like agrin, phosphacan and N-cadherin, whose lysis permits deconstruction of injured synapses prior their reorganization. During the subsequent regenerative phase, OPN positive microglia align along the intact/deafferented border, where matrix proteins like agrin can form a boundary to guide regenerating fibers (Falo et al., 2008). OPN may then act as a microglial-secreted astrokine, inducing astrocytes to produce molecules which support new synaptic regrowth (Ellison et al., 1999). Further studies of these later regenerative phases are needed to confirm OPN astrokine role during TBI synaptogenesis. It should be noted that OPN expression is not limited to supportive glia, but may also be present within neurons (Ju et al., 2000; Higo et al., 2010; Misawa et al., 2012). While we did not observe UEC effect on neuronal OPN, the cytokine has been reported to increase within cortical neurons after CNS

trauma (Borges et al., 2008; Park et al., 2012; Yamamoto et al., 2013) and with neurodegenerative disease (Wung et al., 2007; Maetzler et al., 2006).

Immune suppression and genetic KO also support OPN-mediated regulation of synaptogenesis. Post-UEC minocycline reduced OPN expression, microglial redistribution, MMP-9 activity and OPN fragment production, all correlated with abnormal removal of degenerating synapsin-1 positive axons. Such OPN reduction was predicted, given minocycline attenuation of TBI cytokine elevation (Sanchez Mejia et al., 2001; Crack et al., 2009). However, the drug also inhibits regeneration (Keilhoff et al., 2007) supporting our finding that acute OPN reduction slows down recovery. We also found evidence indicating MMP-9 generation of OPN fragments critical to integrin mediated cell response (Takafuji et al., 2007). While minocycline effects support MMP-9 OPN processing to signal early synaptic reorganization, immunosuppression is not ideal for testing this mechanism since it can alter cell death, free radical generation and MMP activation (Matsukawa et al., 2009; Zhu et al., 2002; Brundula et al., 2002; Power et al., 2003; Machado et al., 2006). Interestingly, OPN KO mice subjected to UEC show acute degenerative/regenerative response similar to that following UEC+minocycline. Lower KO MMP-9 activity and synapsin-1 degradation supports OPN mediation of axonal clearance. Further, attenuated KO MMP-9 activity was spatially and temporally correlated with reduction of MMP-9 ligand and activator LCN2, suggesting involvement of a LCN2/MMP-9/OPN pathway. KO also attenuated microglial reactivity and alignment, like that seen with Parkinsonian microglial response in OPN KOs subjected to MPTP (Maetzler et al., 2007). OPN appears to preferentially alter presynaptic sites since breakdown of synapsin-1 in the KO did change, but MAP1B and N-cadherin, marking dendritic cytoarchitecture and junction adhesion, did not. Since synapsin supports presynaptic contact (Han et al., 1991; Melloni et al., 1994), its lysis should accompany axon removal. Interestingly, OPN/synaptic interaction exists in schizophrenia, where aberrant hypothalamic connectivity maps with altered OPN (Guest et al., 2012). It should be noted that lack of KO effect on MAP1B and N-cadherin could be due to survival interval examined, since expression of each protein is more fluid during later degeneration/regeneration transition (Popa-Wagner et al., 1999; Takeichi and Abe, 2005).

While impaired motor recovery was reported in OPN KOs with SCI (Hashimoto et al., 2007), our study is the first to document OPN effect on time dependent cognitive recovery, a functional correlate of synaptogenesis (Steward, 1989). Uninjured OPN KOs performed the NOR task as efficiently as WT, but after UEC, KOs exhibited deficits 4–21 days after injury, the period during which functional synapses re-emerge (Reeves and Steward, 1986). Thus, rapid OPN postinjury elevation appears to be important for progression of the time dependent tissue changes underlying functional synaptic plasticity. Attenuated KO synapsin-1 breakdown is also consistent with slower, variable cognitive recovery. Synapsin-1 and behavioral recovery have been correlated after TBI (Wu et al., 2011; Griesbach et al., 2009), a reasonable observation since the efficacy of LTP is altered with persistent presynaptic cleaved synapsin-1 (Sato et al., 2000). Alternatively, OPN could recruit activated T-lymphocytes, influencing behavioral recovery. T-cells affect memory acquisition (Ziv et al., 2006), and OPN KO would dampen T-cell response, a marker of impaired cognition (Derecki et al., 2010). Overall, it appears that when the brain is challenged by injury, rapid increase in OPN supports functional recovery.

Interestingly, OPN KOs achieved NOR recovery 28d postinjury, suggesting compensation in hippocampal circuitry over time. Other cognitive tests (e.g., Barnes Maze, Morris Water Maze) and longer postinjury intervals are needed to confirm the extent and persistence of such recovery. In addition, NOR performance did not change for injured WT mice, but trended toward deficit at 21d. This pattern is likely the result of normal cytokine expression within intact contralateral hippocampus, consistent with more efficient UEC cognitive recovery (Steward et al., 1977). Notably, similar 21d reduction in NOR performance was observed after unilateral cortical impact injury (Han et al., 2011). It is also possible that the 21d shift results from reduced task attention or extensive synaptic pruning at that time. Synaptic electrophysiology and ultrastructural analysis will be required to identify cell substrates underlying these behavioral effects.

In summary, OPN is responsive to CNS deafferentation, a cytokine influencing evolution of synapse reorganization. OPN likely mediates microglial activation and migration through its integrin signaling fragments, supporting degeneration/regeneration transition. Generation of OPN fragments is consistent with MMP-9 activation by LCN2. Since CNS inflammation can be detrimental and beneficial, and OPN pleiotropic in its action (Suzuki et al., 2010b; Degos et al., 2013), understanding how OPN affects TBI synaptogenesis will be imperative for design of immunosuppressant therapies.

Acknowledgements

This work was supported by NIH awards NS 044372, NS 056247 and NS 057758. We thank Lesley Harris, Raiford Black, Nancy Lee and Terry Smith for excellent technical assistance and Dr. Adele Doperalski for helpful comments on the manuscript. The authors are grateful for the expert support and data analysis in the qtRT-PCR studies provided by Tana Blevins and Dr. Catherine Dumur, Molecular Diagnostic Services Laboratory, Department of Pathology, VCU.

References

Baratz R, Tweedie D, Rubovitch V, Luo W, Yoon JS, Hoffer BJ, Greig NH, Pick CG. Tumor necrosis factor-alpha synthesis inhibitor, 3,6'-dithiothalidomide, reverses behavioral impairments induced by minimal traumatic brain injury in mice. J. Neurochem. 2011; 118:1032–1042. [PubMed: 21740439]

Belanger M, Magistretti PJ. The role of astroglia in neuroprotection. Dialogues Clin. Neurosci. 2009; 11:281–295.

Borges K, Gearing M, Rittling S, Sorensen ES, Kotloski R, Denhardt DT, Dingledine R. Characterization of osteopontin expression and function after status epilepticus. Epilepsia. 2008:1675–1685. [PubMed: 18522644]

Bye N, Habgood MD, Callaway JK, Malakooti N, Potter A, Kossmann T, Morganti-Kossmann MC. Transient neuroprotection by minocycline following traumatic brain injury is associated with attenuated microglial activation but no changes in cell apoptosis or neutrophil infiltration. Exp. Neurol. 2007; 204:220–233. [PubMed: 17188268]

Cayabyab FS, Gowribai K, Walz W. Involvement of matrix metalloproteinases-2 and −9 in the formation of a lacuna-like cerebral cavity. J. Neurosci. Res. 2013; 91:920–933. [PubMed: 23606560]

Cernak I, Merkle AC, Koliatsos VE, Bilik JM, Luong QT, Mahota TM, Xu L, Slack N, Windle D, Ahmed FA. The pathobiology of blast injuries and blast-induced neurotrauma as identified using a new experimental model of injury in mice. Neurobiol. Dis. 2011; 41:538–551. [PubMed: 21074615]

Chabas D, Baranzini SE, Mitchell D, Bernard CC, Rittling SR, Denhardt DT, Sobel RA, Lock C, Karpuj M, Pedotti R, Heller R, Oksenberg JR, Steinman L. The influence of the proinflammatory

cytokine, osteopontin, on autoimmune demyelinating disease. Science. 2001; 294:1731–1735. [PubMed: 11721059]

Choi JS, Kim HY, Cha JH, Choi JY, Lee MY. Transient microglial and prolonged astroglial upregulation of osteopontin following transient forebrain ischemia in rats. Brain Res. 2007; 1151:195–202. [PubMed: 17395166]

Choi JS, Cha JH, Park HJ, Chung JW, Chun MH, Lee MY. Transient expression of osteopontin mRNA and protein in amoeboid microglia in developing rat brain. Exp. Brain Res. 2004; 154:275–280. [PubMed: 14557908]

Correale J, Villa A. The neuroprotective role of inflammation in nervous system injuries. J. Neurol. 2004; 251:1304–1316. [PubMed: 15592725]

Crack PJ, Gould J, Bye N, Ross S, Ali U, Habgood MD, Morganti-Kossman C, Saunders NR, Hertzog PJ. Victorian Neurotrauma Research Group. The genomic profile of the cerebral cortex after closed head injury in mice: Effects of minocycline. J. Neural. Transm. 2009; 116:1–12. [PubMed: 19018450]

Csuka E, Morganti-Kossmann MC, Lenzlinger PM, Joller H, Trentz O, Kossman T. IL-10 levels in cerebrospinal fluid and serum of patients with severe traumatic brain injury: Relationship to IL-6, TNF-alpha, TGF-beta1 and blood-brain barrier function. J, Neuroimmunol. 1999; 101:211–221. [PubMed: 10580806]

Cunningham LA, Wetzel M, Rosenberg GA. Multiple roles for MMPs and TIMPs in cerebral ischemia. Glia. 2005; 50:329–339. [PubMed: 15846802]

Dalle Lucca JJ, Chavko M, Dubick MA, Adeeb S, Falabella MJ, Slack JL, McCarron R, Li Y. Blast-induced moderate neurotrauma (BINT) elicits early complement activation and tumor necrosis factor alpha (TNFalpha) release in a rat brain. J. Neurol. Sci. 2012; 318:146–154. [PubMed: 22537900]

Degos V, Maze M, Vacas S, Hirsch J, Guo Y, Shen F, Jun K, van Rooijen N, Gressens P, Young WL, Su H. Bone fracture exacerbates murine ischemic cerebral injury. Anesthesiology. 2013; 118:1362–1372. [PubMed: 23438676]

del Zoppo GJ, Frankowski H, Gu Y-H, Osada T, Kanazawa M, Milner R, Wang X, Hosomi N, Mabuchi T, Koziol JA. Microglial cell activation is a source of metalloproteinase generation during hemorrhagic transformation. J. Cerebr. Blood Flow Metab. 2012; 32:919–932.

Derecki NC, Cardani AN, Yang CH, Quinnies KM, Crihfield A, Lynch KR, Kipnis J. Regulation of learning and memory by meningeal immunity: A key role for IL-4. J. Exp. Med. 2010; 207:1067–1080. [PubMed: 20439540]

Dityatev A, Schachner M. The extracellular matrix and synapses. Cell Tissue Res. 2006; 326:647–654. [PubMed: 16767406]

Dityatev A, Schachner M. Extracellular matrix molecules and synaptic plasticity. Nat. Rev. Neurosci. 2003; 4:456–468. [PubMed: 12778118]

Dixon CE, Lyeth BG, Povlishock JT, Findling RL, Hamm RJ, Marmarou A, Young HF, Hayes RL. A fluid percussion model of experimental brain injury in the rat. J. Neurosurg. 1987; 67:110–119. [PubMed: 3598659]

Dumur CI, Ladd AC, Wright HV, Penberthy LT, Wilkinson DS, Powers CN, Garrett CT, DiNardo LJ. Genes involved in radiation therapy response in head and neck cancers. Laryngoscope. 2009; 119:91–101. [PubMed: 19117295]

Ellison JA, Barone FC, Feuerstein GZ. Matrix remodeling after stroke. de novo expression of matrix proteins and integrin receptors. Ann. N. Y. Acad. Sci. 1999; 890:204–222. [PubMed: 10668427]

Ellison JA, Velier JJ, Spera P, Jonak ZL, Wang X, Barone FC, Feuerstein GZ. Osteopontin and its integrin receptor alpha(v)beta3 are upregulated during formation of the glial scar after focal stroke. Stroke. 1998; 29:1698–1706. discussion 1707. [PubMed: 9707214]

Ennaceur A, Delacour J. A new one-trial test for neurobiological studies of memory in rats. 1: Behavioral data. Behav. Brain Res. 1988; 31:47–59. [PubMed: 3228475]

Erb DE, Povlishock JT. Neuroplasticity following traumatic brain injury: A study of GABAergic terminal loss and recovery in the cat dorsal lateral vestibular nucleus. Exp. Brain Res. 1991; 83:253–267. [PubMed: 2022238]

Ethell IM, Ethell DW. Matrix metalloproteinases in brain development and remodeling: Synaptic functions and targets. J. Neurosci. Res. 2007; 85:2813–2823. [PubMed: 17387691]

Falo MC, Reeves TM, Phillips LL. Agrin expression during synaptogenesis induced by traumatic brain injury. J. Neurotrauma. 2008; 25:769–783. [PubMed: 18627255]

Falo MC, Fillmore HL, Reeves TM, Phillips LL. Matrix metalloproteinase-3 expression profile differentiates adaptive and maladaptive synaptic plasticity induced by traumatic brain injury. J. Neurosci. Res. 2006; 84:768–781. [PubMed: 16862547]

Fifre A, Sponne I, Koziel V, Kriem B, Yen Potin FT, Bihain BE, Olivier JL, Oster T, Pillot T. Microtubule-associated protein MAP1A, MAP1B, and MAP2 proteolysis during soluble amyloid beta-peptide-induced neuronal apoptosis. synergistic involvement of calpain and caspase-3. J. Biol. Chem. 2006; 281:229–240. [PubMed: 16234245]

Fuller BF, Cortes DF, Landis MK, Yohannes H, Griffin HE, Stafflinger JE, Bowers MS, Lewis MH, Fox MA, Ottens AK. Exposure of rats to environmental tobacco smoke during cerebellar development alters behavior and perturbs mitochondrial energetics. Environ. Health Perspect. 2012; 120:1684–1691. [PubMed: 23014793]

Goussev S, Hsu J-Y, Lin Y, Tjoa T, Maida N, Werb Z, Noble-Haeusslein LJ. Differential temporal expression of matrix metalloproteinases after spinal cord injury: relationship to revascularization and wound healing. J. Neurosurgery. 2003; 99:188–197.

Greif KF, Trenchard H. Neonatal deafferentation prevents normal expression of synaptic vesicle antigens in the developing rat superior cervical ganglion. Synapse. 1988; 2:1–6. [PubMed: 3138771]

Griesbach GS, Sutton RL, Hovda DA, Ying Z, Gomez-Pinilla F. Controlled contusion injury alters molecular systems associated with cognitive performance. J. Neurosci. Res. 2009; 87:795–805. [PubMed: 18831070]

Guest PC, Urday S, Ma D, Stelzhammer V, Harris LW, Amess B, Pietsch S, Oheim C, Ozanne SE, Bahn S. Proteomic analysis of the maternal protein restriction rat model for schizophrenia: Identification of translational changes in hormonal signaling pathways and glutamate neurotransmission. Proteomics. 2012; 12:3580–3589. [PubMed: 23071080]

Hamby ME, Sofroniew MV. Reactive astrocytes as therapeutic targets for CNS disorders. Neurotherapeutics. 2010; 7:494–506. [PubMed: 20880511]

Han HQ, Nichols RA, Rubin MR, Bahler M, Greengard P. Induction of formation of presynaptic terminals in neuroblastoma cells by synapsin IIb. Nature. 1991; 349:697–700. [PubMed: 1899916]

Han X, Tong J, Zhang J, Farahvar A, Wang E, Yang J, Samadani U, Smith DH, Huang JH. Imipramine treatment improves cognitive outcome associated with enhanced hippocampal neurogenesis after traumatic brain injury in mice. J. Neurotrauma. 2011; 28:995–1007. [PubMed: 21463148]

Hanisch UK. Microglia as a source and target of cytokines. Glia. 2002; 40:140–155. [PubMed: 12379902]

Hardman R, Evans DJ, Fellows L, Hayes B, Rupniak HT, Barnes JC, Higgins GA. Evidence for recovery of spatial learning following entorhinal cortex lesions in mice. Brain Res. 1997; 758:187–200. [PubMed: 9203548]

Hashimoto M, Sun D, Rittling SR, Denhardt DT, Young W. Osteopontin-deficient mice exhibit less inflammation, greater tissue damage, and impaired locomotor recovery from spinal cord injury compared with wild-type controls. J. Neurosci. 2007; 27:3603–3611. [PubMed: 17392476]

Hashimoto M, Koda M, Ino H, Murakami M, Yamazaki M, Moriya H. Upregulation of osteopontin expression in rat spinal cord microglia after traumatic injury. J. Neurotrauma. 2003; 20:287–296. [PubMed: 12820683]

Helmy A, Carpenter KL, Menon DK, Pickard JD, Hutchinson PJ. The cytokine response to human traumatic brain injury: Temporal profiles and evidence for cerebral parenchymal production. J, Cereb, Blood Flow Metab. 2011; 31:658–670. [PubMed: 20717122]

Higo N, Sato A, Yamamoto T, Nishimura Y, Oishi T, Murata Y, Onoe H, Yoshino-Saito K, Tsuboi F, Takahashi M, Isa T, Kojima T. SPP1 is expressed in corticospinal neurons of the macaque sensorimotor cortex. J Comp Neurol. 2010; 518(13):2633–2644. [PubMed: 20503431]

Hwang SM, Lopez CA, Heck DE, Gardner CR, Laskin DL, Laskin JD, Denhardt DT. Osteopontin inhibits induction of nitric oxide synthase gene expression by inflammatory mediators in mouse kidney epithelial cells. J. Biol. Chem. 1994; 269:711–715. [PubMed: 7506262]

Iczkiewicz J, Rose S, Jenner P. Osteopontin (eta-1) is present in the rat basal ganglia. Brain Res. Mol. Brain Res. 2004; 132:64–72. [PubMed: 15548430]

Israelsson C, Lewen A, Kylberg A, Usoskin D, Althini S, Lindeberg J, Deng CX, Fukuda T, Wang Y, Kaartinen V, Mishina Y, Hillered L, Ebendal T. Genetically modified bone morphogenetic protein signaling alters traumatic brain injury-induced gene expression responses in the adult mouse. J, Neurosci. Res. 2006; 84:47–57. [PubMed: 16583403]

John GR, Lee SC, Brosnan CF. Cytokines: Powerful regulators of glial cell activation. Neuroscientist. 2003; 9:10–22. [PubMed: 12580336]

Ju WK, Kim KY, Cha JH, Kim IB, Lee MY, Oh SJ, Chung JW, Chun MH. Ganglion cells of the rat retina show osteopontin-like immunoreactivity. Brain Res. 2000; 852(1):217–220. [PubMed: 10661516]

Kang WS, Choi JS, Shin YJ, Kim HY, Cha JH, Lee JY, Chun MH, Lee MY. Differential regulation of osteopontin receptors, CD44 and the alpha(v) and beta(3) integrin subunits, in the rat hippocampus following transient forebrain ischemia. Brain Res. 2008; 1228:208–216. [PubMed: 18638458]

Keilhoff G, Langnaese K, Wolf G, Fansa H. Inhibiting effect of minocycline on the regeneration of peripheral nerves. Dev. Neurobiol. 2007; 67:1382–1395. [PubMed: 17638380]

Kelso ML, Scheff NN, Scheff SW, Pauly JR. Melatonin and minocycline for combinatorial therapy to improve functional and histopathological deficits following traumatic brain injury. Neurosci. Lett. 2011; 488:60–64. [PubMed: 21056621]

Kim HJ, Fillmore HL, Reeves TM, Phillips LL. Elevation of hippocampal MMP-3 expression and activity during trauma-induced synaptogenesis. Exp. Neurol. 2005; 192:60–72. [PubMed: 15698619]

Kloss CU, Werner A, Klein MA, Shen J, Menuz K, Probst JC, Kreutzberg GW, Raivich G. Integrin family of cell adhesion molecules in the injured brain: Regulation and cellular localization in the normal and regenerating mouse facial motor nucleus. J. Comp. Neurol. 1999; 411:162–178. [PubMed: 10404114]

Knoblach SM, Faden AI. Interleukin-10 improves outcome and alters proinflammatory cytokine expression after experimental traumatic brain injury. Exp. Neurol. 1998; 153:143–151. [PubMed: 9743576]

Kumar A, Stoica BA, Sabirzhanov B, Burns MP, Faden AI, Loane DJ. Traumatic brain injury in aged animals increases lesion size and chronically alters microglial/macrophage classical and alternative activation states. Neurobiol. Aging. 2013; 34:1397–1411. [PubMed: 23273602]

Lee MY, Shin SL, Choi YS, Kim EJ, Cha JH, Chun MH, Lee SB, Kim SY. Transient upregulation of osteopontin mRNA in hippocampus and striatum following global forebrain ischemia in rats. Neurosci. Lett. 1999; 271:81–84. [PubMed: 10477107]

Liaw L, Birk DE, Ballas CB, Whitsitt JS, Davidson JM, Hogan BL. Altered wound healing in mice lacking a functional osteopontin gene (spp1). J. Clin. Invest. (UNITED STATES). 1998; 101:1468–1478.

Lively S, Schlichter LC. The microglial activation state regulates migration and roles of matrix-dissolving enzymes for invasion. J. Neuroinflam. 2013; 10:75–88.

Loesche J, Steward O. Behavioral correlates of denervation and reinnervation of the hippocampal formation of the rat: Recovery of alternation performance following unilateral entorhinal cortex lesions. Brain Res. Bull. 1977; 2:31–39. [PubMed: 861769]

Long P, Samnakay P, Jenner P, Rose S. A yeast two-hybrid screen reveals that osteopontin associates with MAP1A and MAP1B in addition to other proteins linked to microtubule stability, apoptosis and protein degradation in the human brain. Eur. J. Neurosci. 2012; 36:2733–2742. [PubMed: 22779921]

Lu L, Tonchev AB, Kaplamadzhiev DB, Boneva NB, Mori Y, Sahara S, Ma D, Nakaya MA, Kikuchi M, Yamashima T. Expression of matrix metalloproteinases in the neurogenic niche of the adult monkey hippocampus after ischemia. Hippocampus. 2008; 18:1074–1084. [PubMed: 18566964]

Lund RD, Lund JS. Synaptic adjustment after deafferentation of the superior colliculus of the rat. Science. 1971; 171:804–807. [PubMed: 5549304]

Machado LS, Kozak A, Ergul A, Hess DC, Borlongan CV, Fagan SC. Delayed minocycline inhibits ischemia-activated matrix metalloproteinases 2 and 9 after experimental stroke. BMC Neurosci. 2006; 7:56. [PubMed: 16846501]

Maetzler W, Berg D, Schalamberidze N, Melms A, Schott K, Mueller JC, Liaw L, Gasser T, Nitsch C. Osteopontin is elevated in parkinson's disease and its absence leads to reduced neurodegeneration in the MPTP model. Neurobiol. Dis. 2007; 25:473–482. [PubMed: 17188882]

Matsukawa N, Yasuhara T, Hara K, Xu L, Maki M, Yu G, Kaneko Y, Ojika K, Hess DC, Borlongan CV. Therapeutic targets and limits of minocycline neuroprotection in experimental ischemic stroke. BMC Neurosci. 2009; 10 126-2202-10-126.

Maetzler W, Berg D, Schalamberidze N, Melms A, Schott K, Mueller JC, Liaw L, Gasser T, Nitsch C. Osteopontin is elevated in Parkinson's disease and its absence leads to reduced neurodegeneration in the MPTP model. Neurobiol Dis. 2007; 25(3):473–482. [PubMed: 17188882]

Melloni RH Jr, Apostolides PJ, Hamos JE, DeGennaro LJ. Dynamics of synapsin I gene expression during the establishment and restoration of functional synapses in the rat hippocampus. Neuroscience. 1994; 58:683–703. [PubMed: 7514766]

Meunier J, Villard V, Givalois L, Maurice T. The gamma-secretase inhibitor 2-[(1R)-1-[(4-chlorophenyl)sulfonyl](2,5-difluorophenyl) amino]ethyl-5-fluorobenzenebutanoic acid (BMS-299897) alleviates Abeta1-42 seeding and short-term memory deficits in the Abeta25-35 mouse model of Alzheimer’s disease. Eur. J. Pharmacol. 2001; 698:193–199. [PubMed: 23123349]

Milner R, Campbell IL. The integrin family of cell adhesion molecules has multiple functions within the CNS. J. Neurosci. Res. 2002; 69:286–291. [PubMed: 12125070]

Misawa H, Hara M, Tanabe S, Niikura M, Moriwaki Y, Okuda T. Osteopontin is an alpha motor neuron marker in the mouse spinal cord. J Neurosci Res. 2012:732–742. [PubMed: 22420030]

Moon C, Heo S, Ahn M, Kim H, Shin M, Sim KB, Kim HM, Shin T. Immunohistochemical study of osteopontin in the spinal cords of rats with clip compression injury. J. Vet. Med. Sci. 2004; 66:1307–1310. [PubMed: 15528873]

Morganti-Kossmann MC, Rancan M, Stahel PF, Kossmann T. Inflammatory response in acute traumatic brain injury: A double-edged sword. Curr. Opin. Crit. Care. 2002; 8:101–105. [PubMed: 12386508]

Morita M, Imai H, Liu Y, Xu X, Sadamatsu M, Nakagami R, Shirakawa T, Nakano K, Kita Y, Yoshida K, Tsunashima K, Kato N. FK506-protective effects against trimethyltin neurotoxicity in rats: Hippocampal expression analyses reveal the involvement of periarterial osteopontin. Neuroscience. 2008; 153:1135–1145. [PubMed: 18440706]

Nikonenko I, Toni N, Moosmayer M, Shigeri Y, Muller D, Sargent Jonesm L. Integrins are involved in synaptogenesis, cell spreading, and adhesion in the postnatal brain. Brain Res. Dev. Brain Res. 2003; 140:185–194.

Park KP, Rosell A, Foerch C, Xing C, Kim WJ, Lee S, Opdenakker G, Furie KL, Lo EH. Plasma and brain matrix metalloproteinase-9 after acute focal cerebral ischemia in rats. Stroke. 2009; 40:2836–2842. [PubMed: 19556529]

Park JM, Shin YJ, Kim HL, Cho JM, Lee MY. Sustained expression of osteopontin is closely associated with calcium deposits in the rat hippocampus after transient forebrain ischemia. J Histochem Cytochem. 2012; 60(7):550–559. [PubMed: 22496158]

Patarca R, Freeman GJ, Singh RP, Wei FY, Durfee T, Blattner F, Regnier DC, Kozak CA, Mock BA, Morse HC3rd. Structural and functional studies of the early T lymphocyte activation 1 (eta-1) gene. definition of a novel T cell-dependent response associated with genetic resistance to bacterial infection. J. Exp. Med. 1989; 170:145–161. [PubMed: 2787378]

Pellerin L, Magistretti PJ. Neuroenergetics: Calling upon astrocytes to satisfy hungry neurons. Neuroscientist. 2004; 10:53–62. [PubMed: 14987448]

Phillips LL, Lyeth BG, Hamm RJ, Povlishock JT. Combined fluid percussion brain injury and entorhinal cortical lesion: A model for assessing the interaction between neuroexcitation and deafferentation. J. Neurotrauma. 1994; 11:641–656. [PubMed: 7723064]

Plantman S. Osteopontin is upregulated after mechanical brain injury and stimulates neurite growth from hippocampal neurons through beta1 integrin and CD44. Neuroreport. 2012; 23:647–652. [PubMed: 22692550]

Popa-Wagner A, Schroder E, Schmoll H, Walker LC, Kessler C. Upregulation of MAP1B and MAP2 in the rat brain after middle cerebral artery occlusion: Effect of age. J. Cereb. Blood Flow Metab. 1999; 19:425–434. [PubMed: 10197512]

Povlishock JT, Katz DI. Update of neuropathology and neurological recovery after traumatic brain injury. J. Head Trauma Rehabil. 2005; 20:76–94. [PubMed: 15668572]

Power C, Henry S, Del Bigio MR, Larsen PH, Corbett D, Imai Y, Yong VW, Peeling J. Intracerebral hemorrhage induces macrophage activation and matrix metalloproteinases. Ann. Neurol. 2003; 53:731–742. [PubMed: 12783419]

Reeves TM, Steward O. Emergence of the capacity for LTP during reinnervation of the dentate gyrus: Evidence that abnormally shaped spines can mediate LTP. Exp. Brain Res. 1986; 65:167–175. [PubMed: 3803502]

Rothwell NJ, Luheshi GN. Interleukin 1 in the brain: Biology, pathology and therapeutic target. Trends Neurosci. 2000; 23:618–625. [PubMed: 11137152]

Ruoslahti E. Brain extracellular matrix. Glycobiology. 1996a; 6:489–492. [PubMed: 8877368]

Sanchez Mejia RO, Ona VO, Li M, Friedlander RM. Minocycline reduces traumatic brain injury-mediated caspase-1 activation, tissue damage, and neurological dysfunction. Neurosurgery. 2001; 48:1393–1399. discussion 1399-401. [PubMed: 11383749]

Sato K, Morimoto K, Suemaru S, Sato T, Yamada N. Increased synapsin I immunoreactivity during long-term potentiation in rat hippocampus. Brain Res. 2000; 872:219–222. [PubMed: 10924697]

Scatena M, Liaw L, Giachelli M. Osteopontin: A multifunctional molecule regulating chronic inflammation and vascular disease. Arterioscler. Thrombo. Vasc. Biol. 2007; 27:2302–2309.

Shin T, Ahn M, Kim H, Moon C, Kang TY, Lee JM, Sim KB, Hyun JW. Temporal expression of osteopontin and CD44 in rat brains with experimental cryolesions. Brain Res. 2005; 1041:95–101. [PubMed: 15804504]

Shin YJ, Kim HL, Choi JS, Choi JY, Cha JH, Lee MY. Osteopontin: Correlation with phagocytosis by brain macrophages in a rat model of stroke. Glia. 2011; 59:413–423. [PubMed: 21264948]

Shohami E, Gallily R, Mechoulam R, Bass R, Ben-Hur T. Cytokine production in the brain following closed head injury: Dexanabinol (HU-211) is a novel TNF-alpha inhibitor and an effective neuroprotectant. J. Neuroimmunol. 1997; 72:169–177. [PubMed: 9042110]

Shohami E, Novikov M, Bass R, Yamin A, Gallily R. Closed head injury triggers early production of TNF alpha and IL-6 by brain tissue. J. Cereb. Blood Flow Metab. 1994; 14:615–619. [PubMed: 8014208]

Silver J, Miller JH. Regeneration beyond the glial scar. Nat. Rev. Neurosci. 2004; 5:146–156. [PubMed: 14735117]

Siopi E, Llufriu-Daben G, Fanucchi F, Plotkine M, Marchand-Leroux C, Jafarian-Tehrani M. Evaluation of late cognitive impairment and anxiety states following traumatic brain injury in mice: The effect of minocycline. Neurosci. Lett. 2012; 511:110–115. [PubMed: 22314279]

Sofroniew MV. Reactive astrocytes in neural repair and protection. Neuroscientist. 2000; 5:400–407.

Steward O. Reorganization of neuronal connections following CNS trauma: Principles and experimental paradigms. J. Neurotrauma. 1989; 6:99–152. [PubMed: 2671393]

Steward O, Loesche J, Horton WC. Behavioral correlates of denervation and reinnervation of the hippocampal formation of the rat: Open field activity and cue utilization following bilateral entorhinal cortex lesions. Brain Res. Bull. 1977; 2:41–48. [PubMed: 861770]

Su J, Gorse K, Ramirez F, Fox MA. Collagen XIX is expressed by interneurons and contributes to the formation of hippocampal synapses. J. Comp. Neurol. 2010; 518:229–253. [PubMed: 19937713]

Suzuki H, Ayer R, Sugawara T, Chen W, Sozen T, Hasegawa Y, Kanamaru K, Zhang JH. Protective effects of recombinant osteopontin on early brain injury after subarachnoid hemorrhage in rats. Crit. Care Med. 2010b; 38:612–618. [PubMed: 19851092]

Takafuji V, Forgue M, Unsworth E, Goldsmith P, Wang XW. An osteopontin fragment is essential for tumor cell invasion in hepatocellular carcinoma. Oncogene. 2007; 26:6361–6371. [PubMed: 17452979]

Takeichi M, Abe K. Synaptic contact dynamics controlled by cadherin and catenins. Trends Cell Biol. 2005; 15:216–221. [PubMed: 15817378]

Tambuyze BR, Casteleyn C, Vergauwen H, Van Cruchten S, Van Ginneken C. Osteopontin alters the functional profile of porcine microglia in vitro. Cell Biol. Int. 2012; 36:1233–1238. [PubMed: 22974008]

Truett GE, Heeger P, Mynatt RL, Truett AA, Walker JA, Warman ML. Preparation of PCR-quality mouse genomic DNA with hot sodium hydroxide and tris (HotSHOT). BioTechniques. 2000; 29(52):54. [PubMed: 10907077]

Tschesche H, Zolzer V, Triebel S, Bartsch S. The human neutrophil lipocalin supports the allosteric activation of matrix metalloproteinases. Eur. J. Biochem. 2001; 268:1918–1928. [PubMed: 11277914]

van Velthoven CT, Heijnen CJ, van Bel F, Kavelaars A. Osteopontin enhances endogenous repair after neonatal hypoxic-ischemic brain injury. Stroke. 2011; 42:2294–2301. [PubMed: 21700938]

Venstrom KA, Reichardt LF. Extracellular matrix. 2: Role of extracellular matrix molecules and their receptors in the nervous system. FASEB J. 1993; 7:996–1003. [PubMed: 8370483]

Verslegers M, Lemmens K, Van Hove I, Moons L. Matrix metalloproteinase-2 and −9 as promising benefactors in development, plasticity and repair of the nervous system. Prog. Neurobiol. 2013; 105:60–78. [PubMed: 23567503]

Vitarbo EA, Chatzipanteli K, Kinoshita K, Truettner JS, Alonso OF, Dietrich WD. Tumor necrosis factor alpha expression and protein levels after fluid percussion injury in rats: The effect of injury severity and brain temperature. Neurosurgery. 2004; 55:416–424. discussion 424-5. [PubMed: 15271250]

von Gertten C, Flores Morales A, Holmin S, Mathiesen T, Nordqvist AC. Genomic responses in rat cerebral cortex after traumatic brain injury. BMC Neurosci. 2005; 6:69. [PubMed: 16318630]

Wang X, Louden C, Yue TL, Ellison JA, Barone FC, Solleveld HA, Feuerstein GZ. Delayed expression of osteopontin after focal stroke in the rat. J. Neurosci. 1998; 18:2075–2083. [PubMed: 9482794]

Warren KM, Reeves TM, Phillips LL. MT5-MMP, ADAM-10, and N-cadherin act in concert to facilitate synapse reorganization after traumatic brain injury. J. Neurotrauma. 2012; 29:1922–1940. [PubMed: 22489706]

Weber GF, Cantor H. The immunology of eta-1/osteopontin. Cytokine Growth Factor Rev. 1996; 7:241–248. [PubMed: 8971479]

Wu A, Ying Z, Gomez-Pinilla F. The salutary effects of DHA dietary supplementation on cognition, neuroplasticity, and membrane homeostasis after brain trauma. J. Neurotrauma. 2011a; 28:2113–2122. [PubMed: 21851229]

Wung JK, Perry G, Kowalski A, Harris PL, Bishop GM, Trivedi MA, Johnson SC, Smith MA, Denhardt DT, Atwood CS. Increased expression of the remodeling- and tumorigenic-associated factor osteopontin in pyramidal neurons of the Alzheimer's disease brain. Curr Alzheimer Res. 2007:67–72. [PubMed: 17316167]

Yamagata M, Weine JA, Sanes JR. Sidekicks: Synaptic adhesion molecules that promote lamina-specific connectivity in the retina. Cell. 2002; 110:649–660. [PubMed: 12230981]

Yamamoto T, Oishi T, Higo N, Murayama S, Sato A, Takashima I, Sugiyama Y, Nishimura Y, Murata Y, Yoshino-Saito K, Isa T, Kojima T. Differential expression of secreted phosphoprotein 1 in the motor cortex among primate species and during postnatal development and functional recovery. PLoS One. 2011; 8(5):e65701. [PubMed: 23741508]

Yrjanheikki J, Keinanen R, Pellikka M, Hokfelt T, Koistinaho J. Tetracyclines inhibit microglial activation and are neuroprotective in global brain ischemia. Proc. Natl. Acad. Sci. U. S. A. 1998; 95:15769–15774. [PubMed: 9861045]

Yrjanheikki J, Tikka T, Keinanen R, Goldsteins G, Chan PH, Koistinaho J. A tetracycline derivative, minocycline, reduces inflammation and protects against focal cerebral ischemia with a wide therapeutic window. Proc. Natl. Acad. Sci. U.S. A. 1999; 96:13496–13500. [PubMed: 10557349]

Zhao C, Fancy SP, ffrench-Constant C, Franklin RJ. Osteopontin is extensively expressed by macrophages following CNS demyelination but has a redundant role in remyelination. Neurobiol Dis. 2008; 31:209–217. [PubMed: 18539470]

Zhu S, Stavrovskaya IG, Drozda M, Kim BY, Ona V, Li M, Sarang S, Liu AS, Hartley DM, Wu DC, Gullans S, Ferrante RJ, Przedborski S, Kristal BS, Friedlander RM. Minocycline inhibits cytochrome c release and delays progression of amyotrophic lateral sclerosis in mice. Nature. 2002; 417:74–78. [PubMed: 11986668]

Ziv Y, Ron N, Butovsky O, Landa G, Sudai E, Greenberg N, Cohen H, Kipnis J, Schwartz M. Immune cells contribute to the maintenance of neurogenesis and spatial learning abilities in adulthood. Nat. Neurosci. 2006; 9:268–275. [PubMed: 16415867]

Highlights

1. Cortical deafferentation produces time-dependent increase in hippocampal osteopontin
2. Osteopontin production by reactive microglia mediates synapse reorganization
3. Loss of osteopontin through immunosuppression or knock out attenuates synapse repair
4. Metalloproteinase lysis of osteopontin supports glial integrin signaling with synaptogenesis
5. Increased lipocalin 2 is correlated with matrix metalloproteinase-9 proteolysis of osteopontin

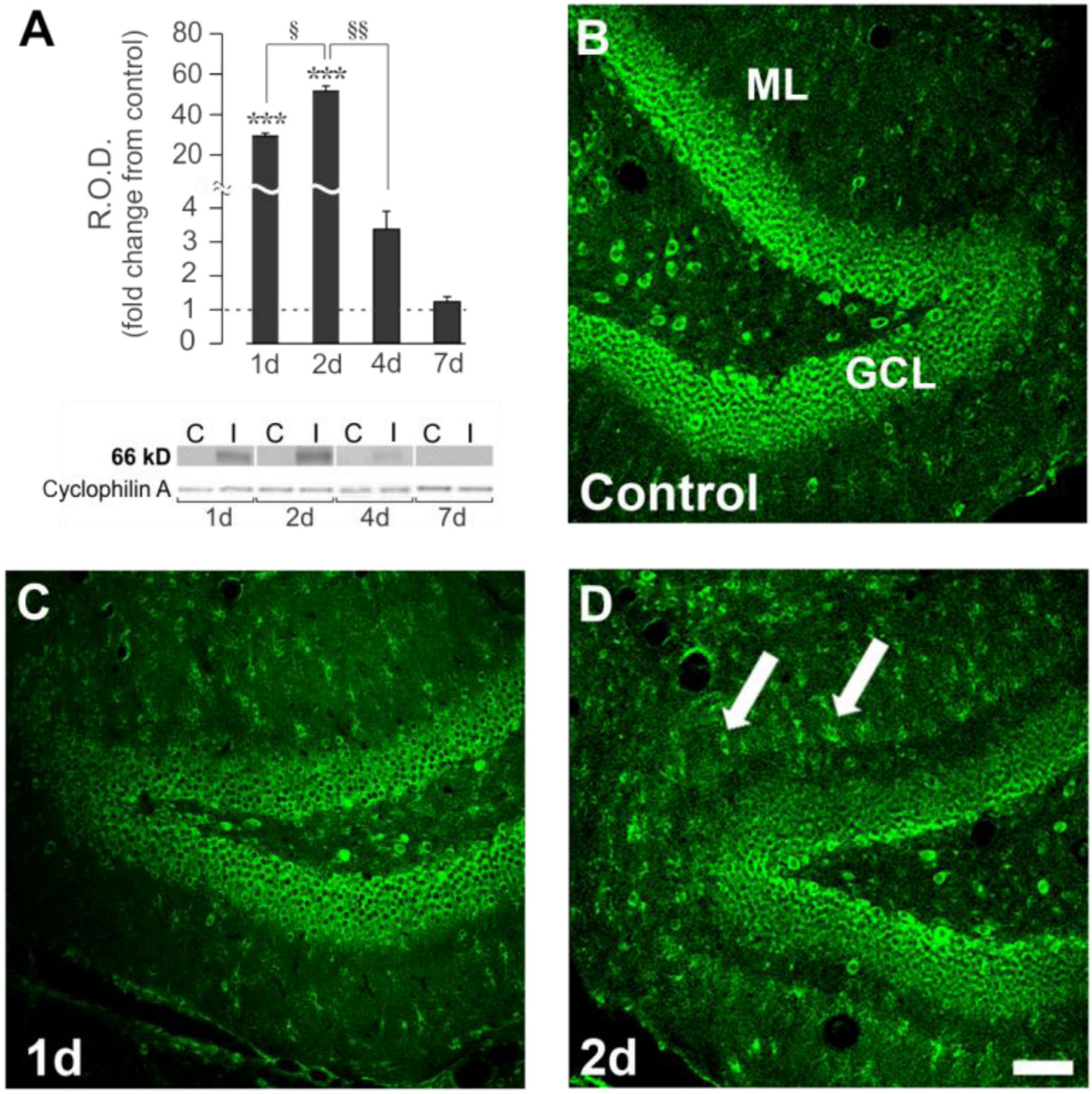

Figure 1. Hippocampal OPN protein expression and distribution during early phases of UEC adaptive synaptogenesis

A. WB showed robust increase of full length (66 kD) hippocampal OPN protein peaking 2d postinjury. OPN at 4d was significantly reduced and approached baseline by 7d. **B.–D**. Confocal imaging shows OPN localized in dentate granule cell laminae (GCL) and molecular layer (ML). OPN increased between 1–2d (**C.,D**.) postinjury in ML, with pronounced signal in small cell bodies (arrows). WB results displayed as fold change over control, with representative blot images and cyclophilin A loading controls below (blot

labels: ‘C’=control; ‘I’=injured). ***p<0.001, relative to paired controls; §p<0.05; §§p<0.01. Scale bar = 75 μm.

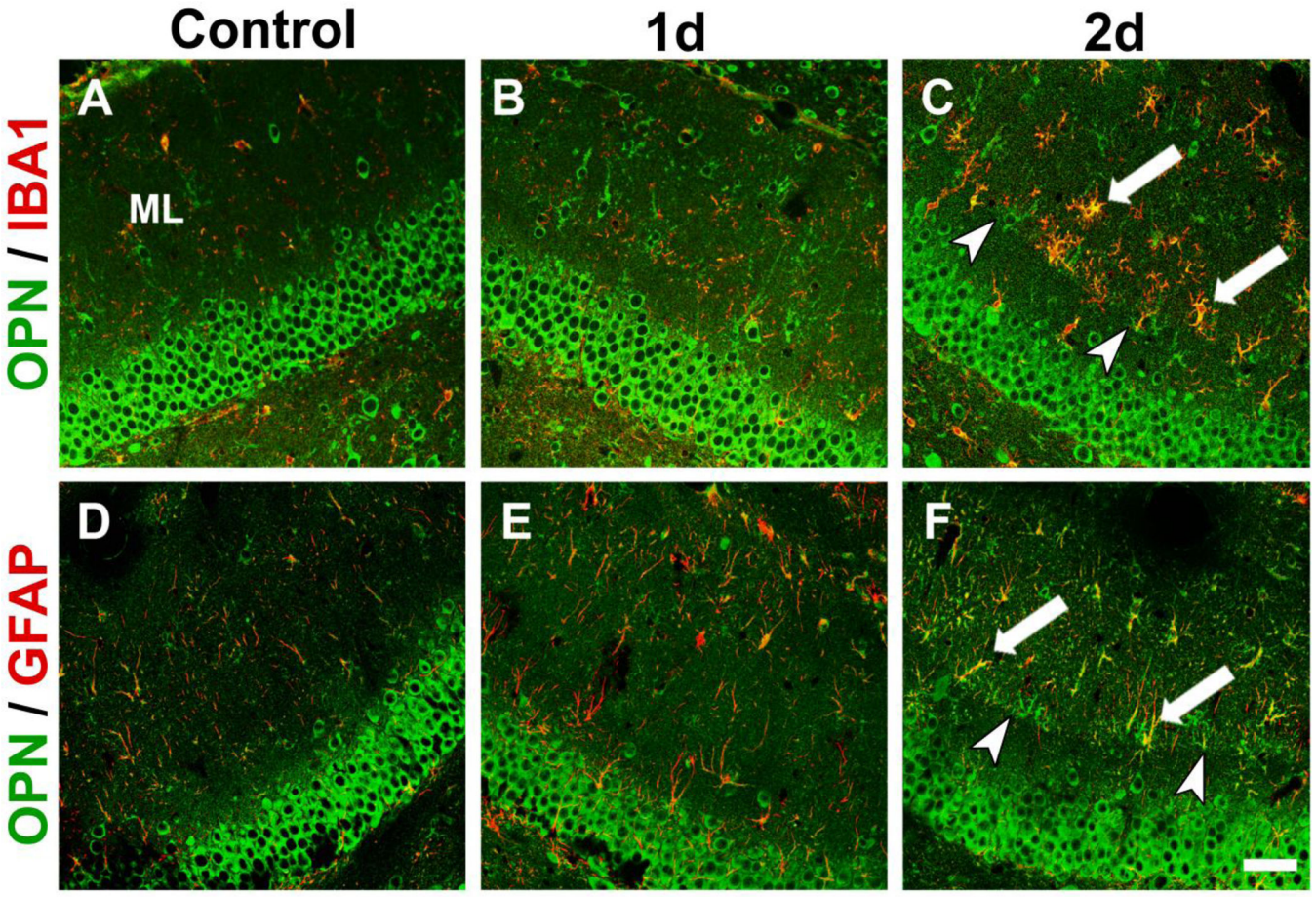

Figure 2. Glial OPN in deafferented dentate gyrus following UEC

Confocal OPN (green) staining is increased over the deafferented ML 1–2d postinjury relative to contralateral control. **A.–C**. Injury-induced OPN co-localized (arrows) with activated microglia (IBA-1 red; OPN green). **D.–F**. Reactive astrocytes (GFAP red; OPN green) also contain OPN. Each cell type showed alignment at intact/deafferented boundary (arrowheads). OPN labeling was most pronounced in 2d reactive microglia. Scale bar = 50 μm.

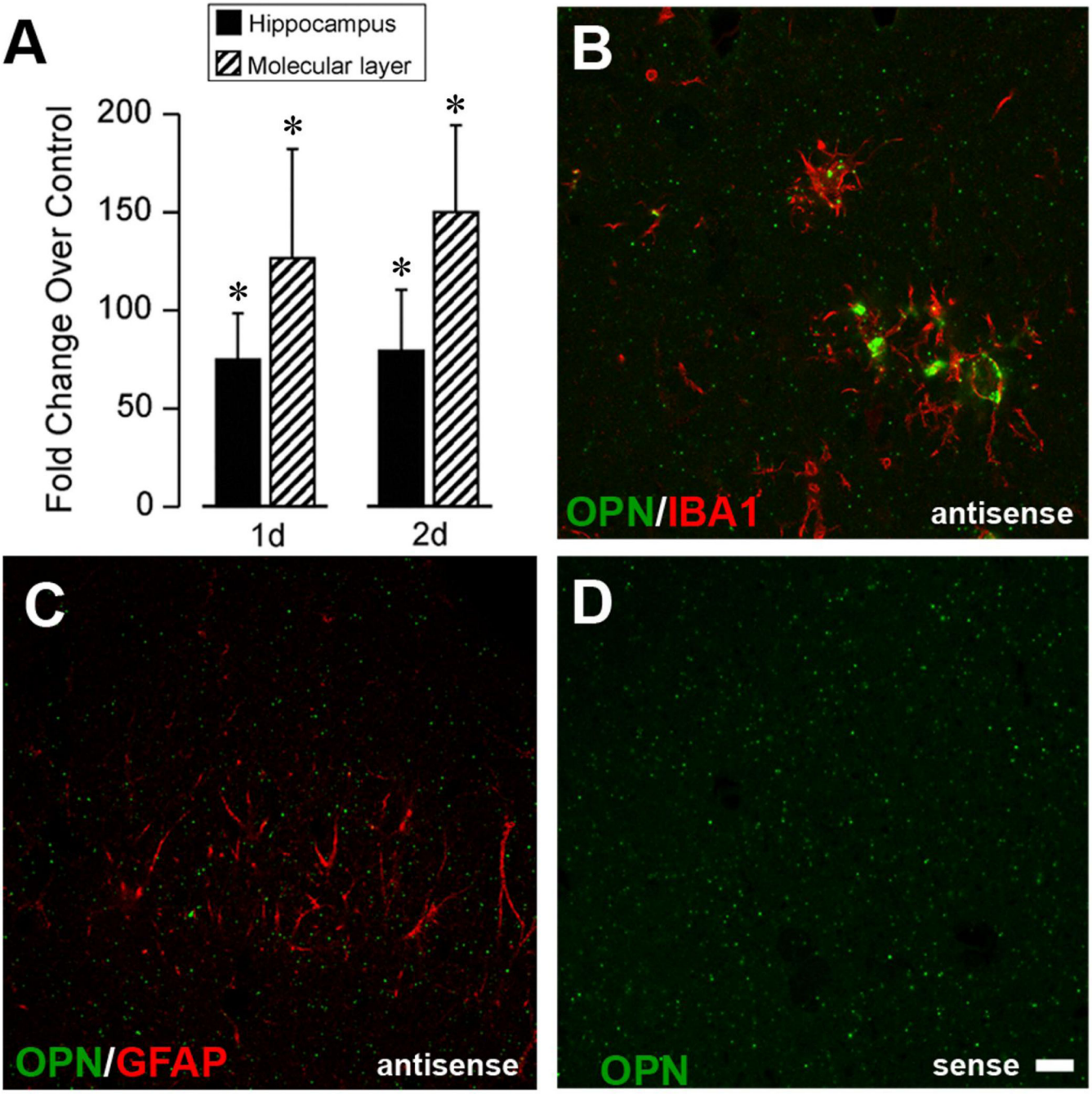

Figure 3. OPN transcript elevation in hippocampus after UEC and localization within microglia of deafferented zone

A. qRT-PCR for hippocampus and ML showed significant OPN transcript elevation 1–2d postinjury. **B**. ISH with antisense DIG-tagged OPN riboprobe (green) revealed ML transcript within activated microglia (red; IBA-1 labeled). **C**. OPN transcript was not localized within GFAP positive astrocytes. **D**. Hybridization validated with sense strand probe. Results are expressed as fold change over control. *p<0.001, relative to paired control cases. Scale bar = 10 μm.

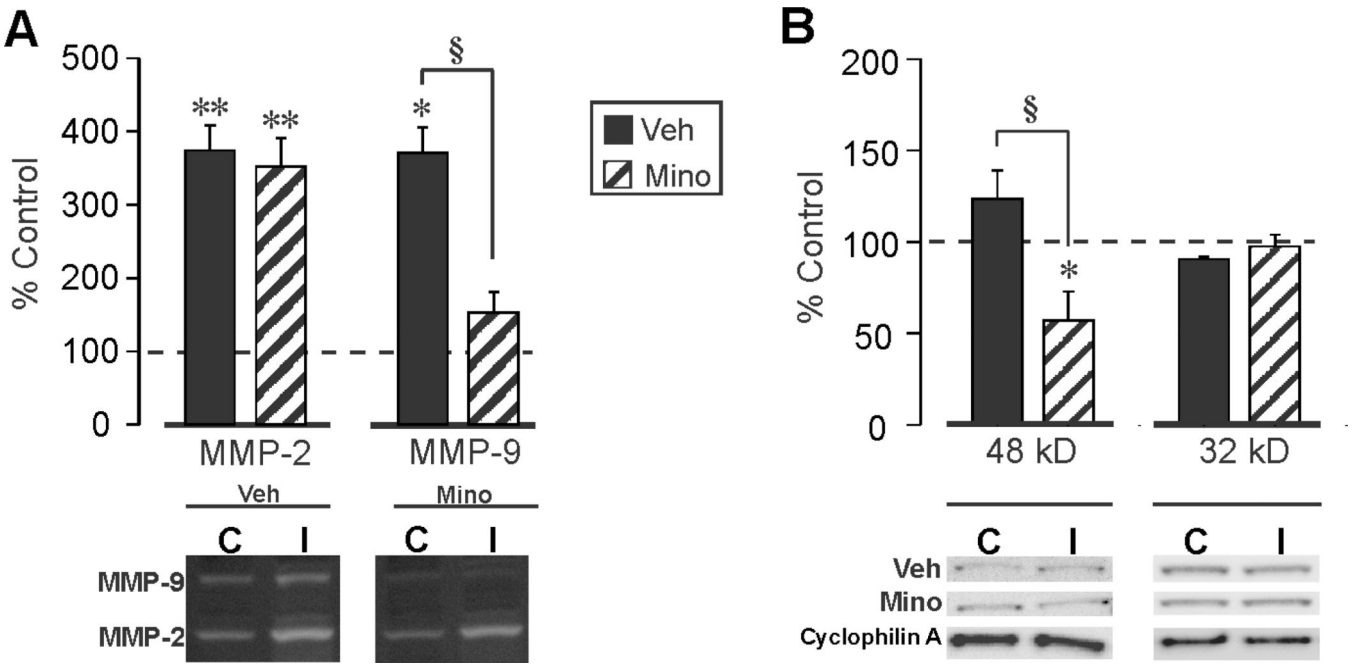

Figure 4. Minocycline attenuation of hippocampal UEC-induced MMP-9 activity and OPN proteolytic fragment generation

A. Zymography revealed elevation in hippocampal MMP-2 and MMP-9 activity 2d after UEC. Minocycline administration selectively reduced MMP-9 proteolysis. **B**. Minocycline-treated samples showed reversal of UEC-induced 48 kD OPN production, suggesting that reduced OPN integrin signaling is correlated with attenuated MMP-9 lysis. Results are displayed as percent change over control with representative blot images and cyclophilin A loading controls below ('C', control; 'I', injured). *$p<0.05$, **$p<0.001$, relative to paired controls; §$p<0.001$.

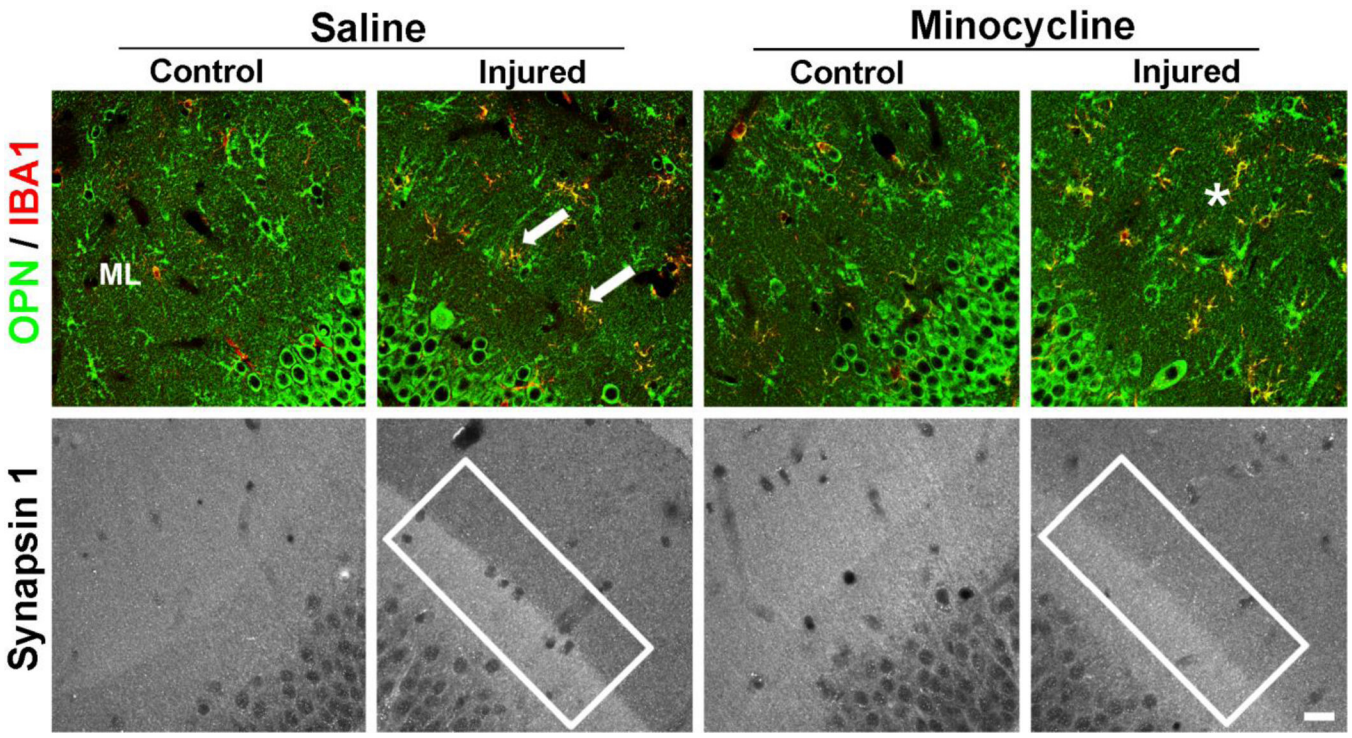

Figure 5. Minocycline effect on alignment of OPN positive glia and presynaptic terminal removal in deafferented molecular layer following UEC

Confocal imaging of minocycline-treated animals 2d after UEC showed a more random distribution of OPN positive neuroglia (green) within the deafferented ML compared with saline vehicle cases (*; top panel). With minocycline, OPN containing microglia (IBA-1, red) were less organized along the intact/deafferented boundary as in controls (arrows). At 2d after UEC, removal of degenerating axon terminals produces a crisp intact/deafferented zone synapsin-1 boundary (box; bottom saline panel). Minocycline results in loss of this sharp boundary and shows synapsin-1 signal extending into the deafferented side, supporting reduced presynaptic terminal clearance (box; bottom minocycline panel). Scale bar = 20 μm.

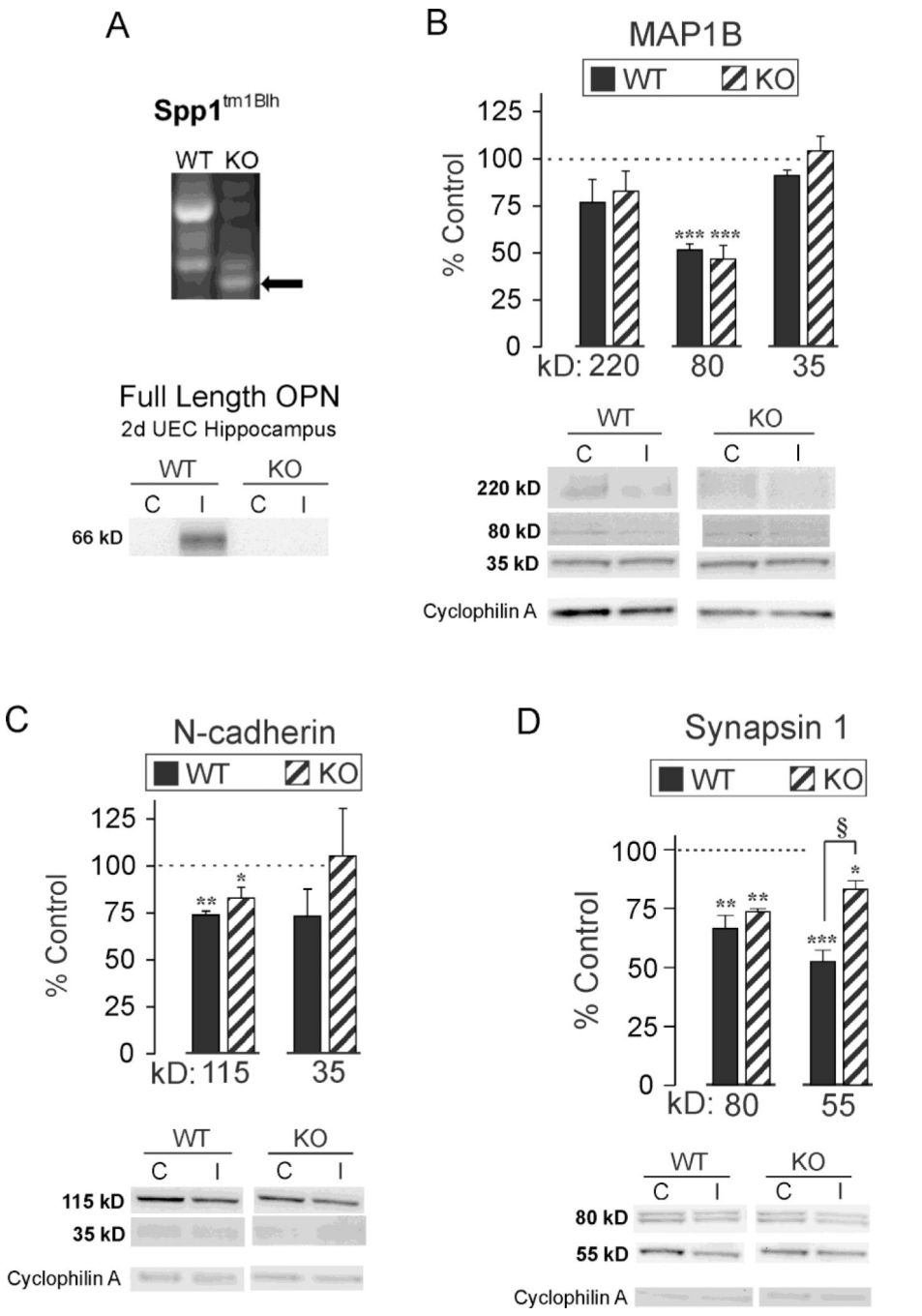

Figure 6. Effect of OPN KO on UEC-induced MAP1B, N-cadherin and synapsin-1 proteolysis

A. RT-PCR confirmation of neo^{r}cassette replacing of exons 4–7 in OPN KOs and OPN protein loss in 2d UEC hippocampus of KO mice. **B**. WB of WT hippocampal MAP1B revealed full length (220 kD) and 80, 35 kD fragments, with significant reduction in the 80 kD fragment 2d after UEC. OPN KO failed to affect postinjury MAP1B expression. **C**. WT full length (115 kD) and 35 kD cleaved N-cadherin were also decreased after UEC, but only the 115 kD reduction reached significance. Similar to MAP1B, OPN KO failed to change N-cadherin response. **D**. The 80 kD full length and 55 kD cysteine cleavage product of

synapsin-1 were reduced for UEC WT, while the injury-induced change in the 55 kD product was significantly attenuated in OPN KO. Results are displayed as percent of uninjured paired control, with representative blot images and cyclophilin A loading controls below ('C', control; 'I', injured). *$p<0.05$, **$p<0.01$, ***$p<0.001$ relative to paired controls; §$p<0.01$.

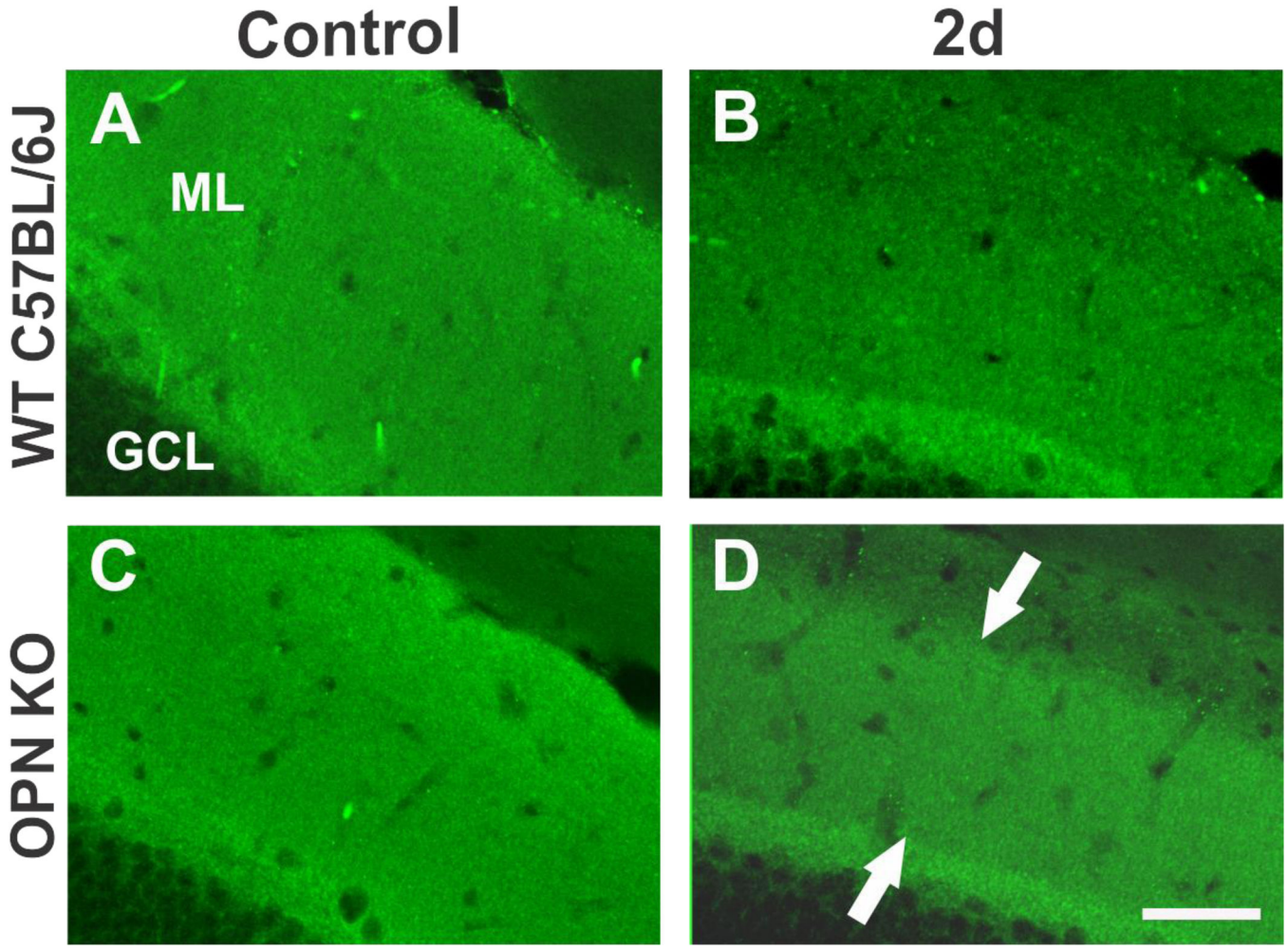

Figure 7. Effect of OPNKO on synapsin-1 distribution within the UEC deafferented dentate molecular layer

A–B. Confocal images of synapsin-1 staining show the predicted pronounced decrease over the WT deafferented zone at 2d postinjury relative to contralateral control ML. **C.–D**. OPN KO mice subjected to UEC showed persistent synapsin-1 localization within a significant portion of the deafferented dentate ML (arrows in **D**.). Scale bar = 50 μm.

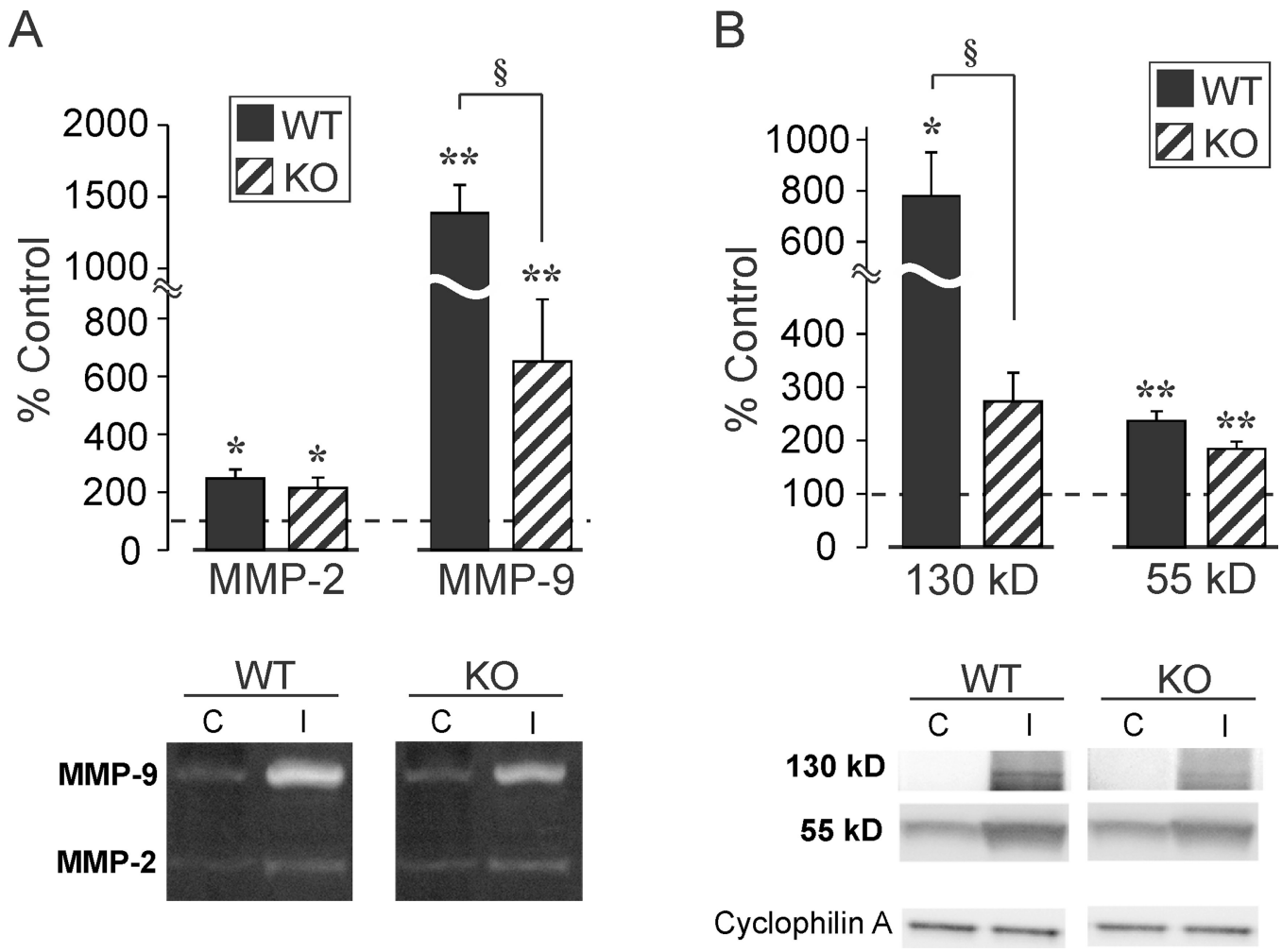

Figure 8. Effect of OPN KO on UEC-induced MMP-9 activity and neutrophil gelatinase-associated lipocalin (LCN2) expression

A. Hippocampal zymography 2d after UEC showed predominant change in MMP-9 activity for both WT and OPN KO. Injury-induced MMP-9 lysis was reduced by 53% in OPN KOs. **B**. In tandem, putative 130 kD enzyme bound form of LCN2 protein robustly increased at 2d postinjury in WT mice. OPN loss attenuated 130 kD LCN2 signal by 65%. Results are expressed as percent of uninjured paired control, with representative gel images below.*p<0.01, **p<0.001 relative to paired controls; §p<0.05.

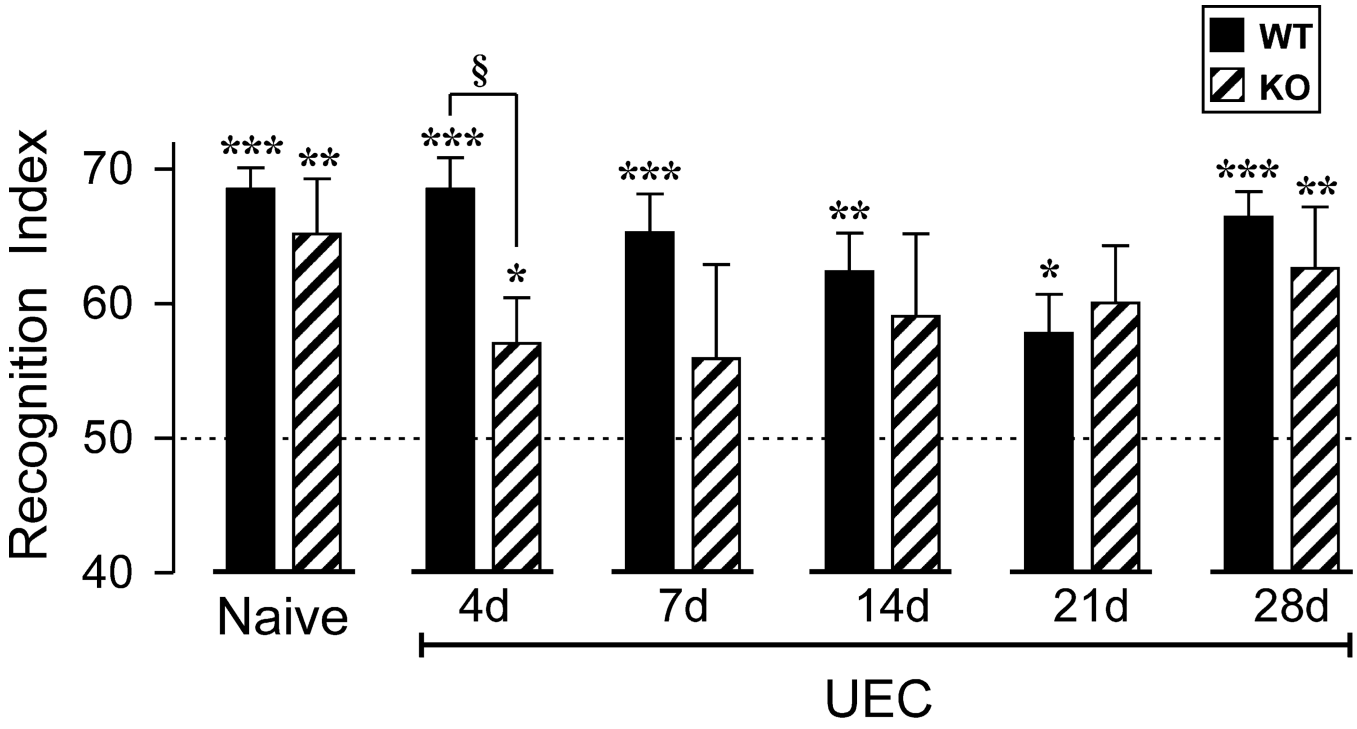

Figure 9. Effect of OPN KO on novel object recognition (NOR) task

Mean recognition index (RI) for NOR performance is plotted for uninjured mice, and for mice tested at 4d-28d post-UEC. Asterisks denote significant recognition of the novel object (RI > 50%): *p<0.05, **p<0.01, ***p<0.001. For WT mice, NOR performance remained significantly above chance levels at all testing days, although there was a delayed reduction in RI, with the worst performance at 21d. In contrast, OPN KO mice performed significantly below WT levels at 4d post-UEC (§p<0.05), and failed to perform significantly above chance levels during the 7d-21d interval. By 28d, similar RI values revealed successful NOR for each strain, suggesting that KO mice had compensated for the earlier signaling deficits.

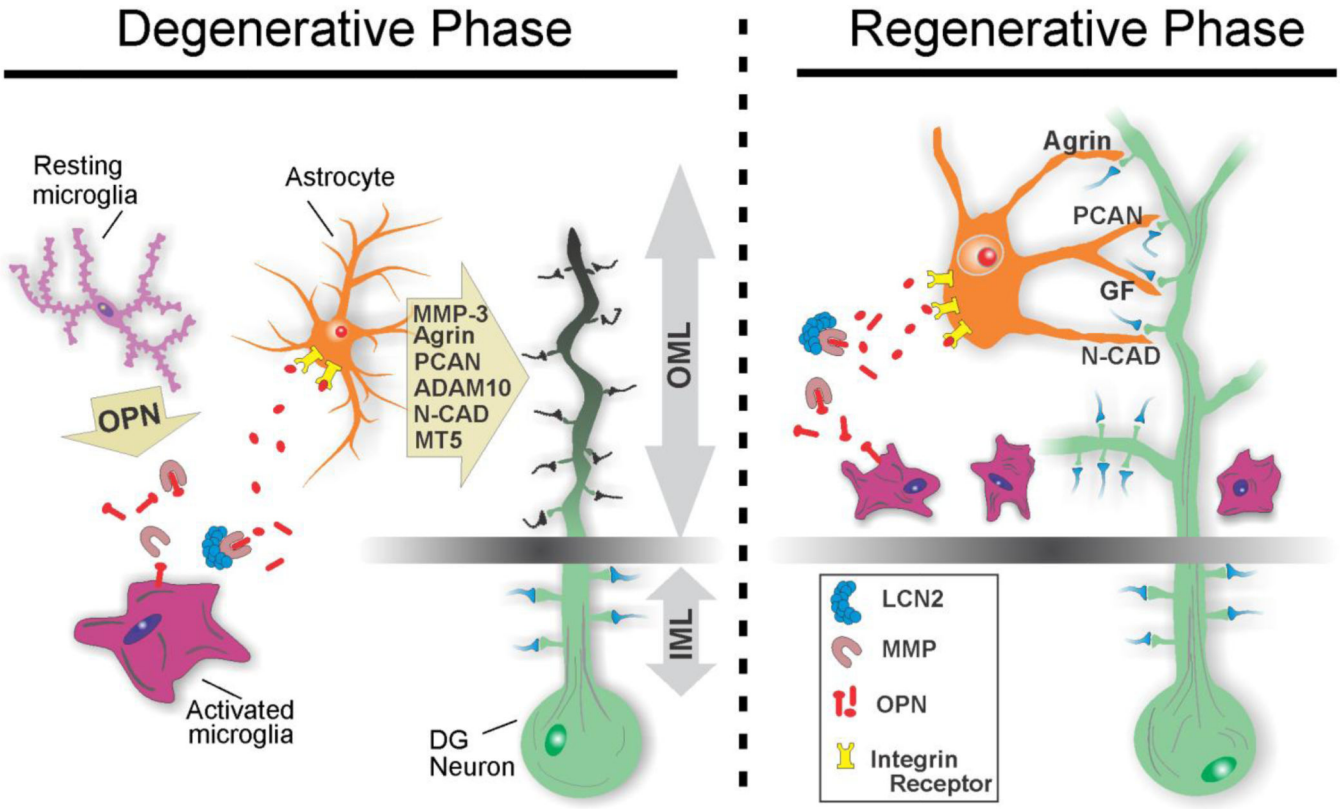

Figure 10. Cellular model of OPN-mediated effects on dentate glia during synaptogenesis

Neuroglial interactions affecting dendritic and synaptic integrity within the deafferented outer molecular layer (OML) are depicted for degenerative and regenerative phases. Rapid postinjury elevation of OPN drives microglial activation from a resting state to a M1 pro-inflammatory form. With axon degeneration, microglia secrete OPN and MMPs, promoting local OPN lysis, facilitated by LCN2/MMP-9 interaction. Astrocytes respond to OPN integrin signaling and elicit ECM-mediated breakdown of synapse stabilizing molecules. This promotes removal of degenerating presynaptic terminals and modification of postsynaptic dendrites prior to synapse reconstruction. During early synapse regeneration, microglia continue to produce OPN and align along the deafferentation boundary, guiding sprouting axons to sites of reinnervation. OPN fragments can again direct astrocyte activation, inducing production and delivery of molecules which support re-emerging synapse structure.